frontiers | Frontiers in Earth Science

TYPE Original Research
PUBLISHED 23 January 2024
DOI 10.3389/feart.2023.1305893

OPEN ACCESS

EDITED BY
Lawrence H. Tanner,
Le Moyne College, United States

REVIEWED BY
Victor Hugo Garcia,
Pontifical Catholic University of Peru, Peru
Giovanni Luca Cardello,
University of Sassari, Italy

*CORRESPONDENCE
Gustavo Martins,
gustavogeologist@gmail.com

RECEIVED 02 October 2023
ACCEPTED 29 December 2023
PUBLISHED 23 January 2024

CITATION
Martins G, Ettensohn FR and Knutsen S-M (2024), Using the tectophase conceptual model to assess late Triassic–Early Jurassic far-field tectonism across the South-central Barents Sea shelf.
Front. Earth Sci. 11:1305893.
doi: 10.3389/feart.2023.1305893

Using the tectophase conceptual model to assess late Triassic–Early Jurassic far-field tectonism across the South-central Barents Sea shelf

Gustavo Martins[1]*, Frank R. Ettensohn[1] and Stig-Morten Knutsen[2,3]

[1]Department of Earth and Environmental Sciences, University of Kentucky, Lexington, KY, United States, [2]Norwegian Petroleum Directorate, Harstad, Norway, [3]Department of Geosciences, UiT—The Arctic University of Norway, Tromsø, Norway

The Upper Triassic–Lower Jurassic succession of the Barents Sea Shelf (BSS) represents one of Europe's most prolific and strategic petroleum systems. This succession reflects various depositional environments and tectonostratigraphic events. Even though these strata are considered largely well-understood, connections with far-field stresses triggered by regional tectonics remain a subject of investigation. This study presents new interpretations that focus on relationships between the stratigraphic succession across the south-central BSS and Triassic–Jurassic Novaya Zemlya compressional tectonics. By applying the "tectophase model," developed in the Appalachian Basin, to analyze this succession, the presence of foreland-basin depozones and associated far-field processes related to compressional tectonics in an adjacent orogen are suggested. This model addresses unconformity development, lithostratigraphic succession, and reactivation of structures. Use of this model suggests far-field tectonostratigraphic responses during two episodes of Novaya Zemlya tectonism, reflected in the coeval BSS stratigraphy. Overall, this tectonostratigraphic study aligns with other research suggesting a Late Triassic inception for Novaya Zemlya compressional tectonism, which influenced larger parts of the BSS through extensive clastic sedimentation, far-field structural reactivation, and flexural responses to deformational loading triggered by tectonics.

KEYWORDS

compressional tectonics, far-field tectonics, foreland-basin system, tectophase model, novaya zemlya tectonism

1 Introduction

The Barents Sea shelf (BSS) is located between northern Norway, northwestern Russia, Svalbard, Franz Joseph Land and Novaya Zemlya (Figures 1A, B), covers approximately 1.4 million km^2, and consists of a complex system of sedimentary basins, platforms, and structural highs (Figure 1B), with substantial hydrocarbon resources (e.g., Doré et al., 2022). In this large province, Upper Triassic to Jurassic prolific reservoirs host strategic hydrocarbon fields (e.g., Snøhvit, Albatross, Goliat, Askellad, Ludlovskaya, and Shtokmanovskaya) (Duran et al., 2013; Polyakova, 2015). In the Norwegian part of the shelf (western BSS, NBSS; Figure 1B), hydrocarbon exploration has been conducted since

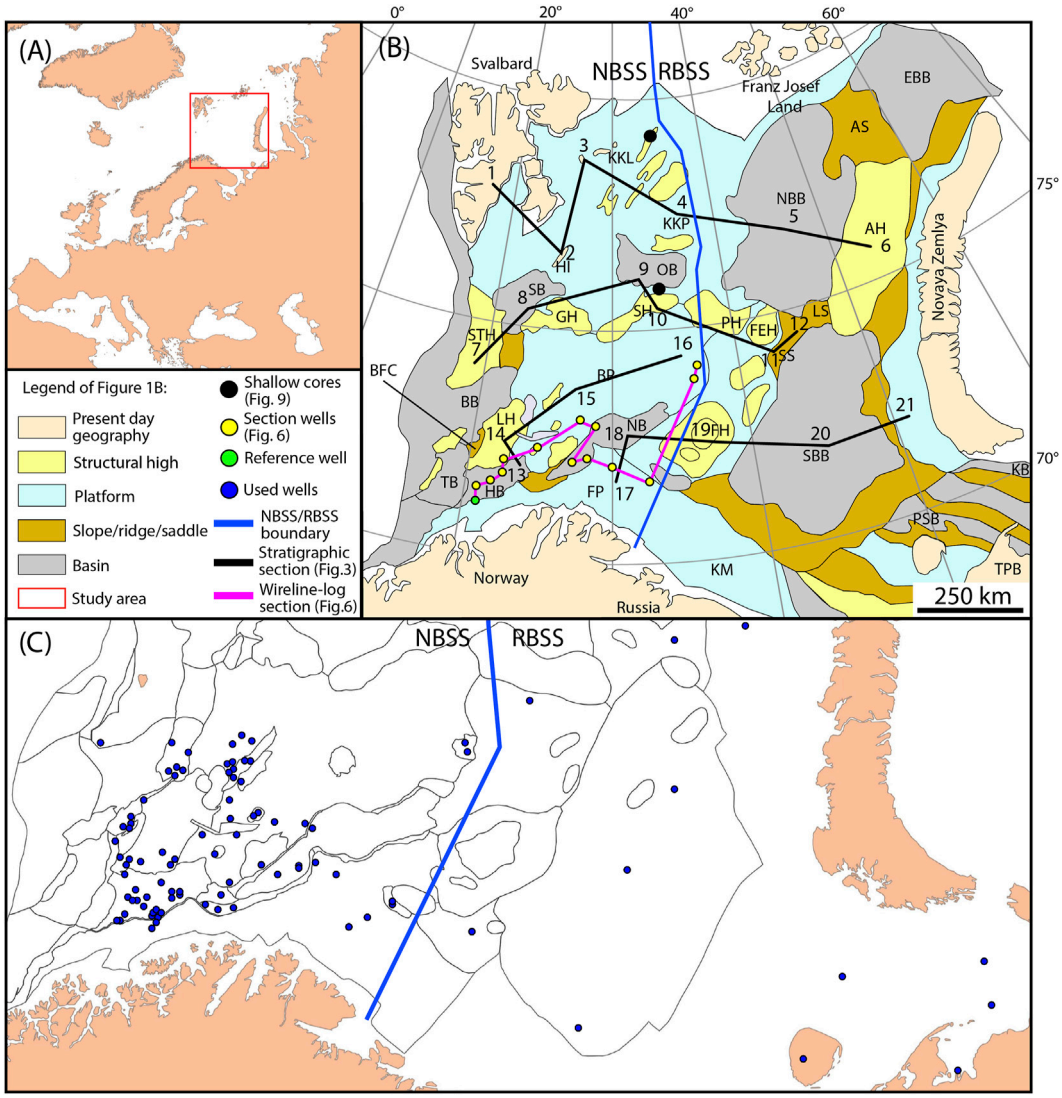

FIGURE 1
(A) Geographic location. **(B)** Main BSS structural elements (adapted from Ryseth, 2014). **(C)** Hydrocarbon exploration well locations used in this study. The grey lines represent the official structural elements in central-southern BSS. Numbers and black lines represent locations of stratigraphic columns and cross sections in Figure 3. The pink line represents a wireline section (Figure 6), which includes the reference well for the Fruholmen Formation (green dot; Dalland et al., 1988). AH=Admiralty High; AS=Albanovskaya Saddle; BB=Bjørnøya Basin; BFC=Bjørnøyrenna Fault Complex; BP=Bjarmeland Platform; EBB=East Barents Basin; FEH=Fersmanovskaya High; FH=Fedinsky High; FP=Finnmark Platform; GH=Gardarbanken High; HB=Hammerfest Basin; HI=Hopen Island; KB=Korothaika Basin; KKL=Kong Karls Land; KKP=Kong Karl Platform; KM=Kola Monocline; LH=Loppa High; LS=Ludlovskaya Saddle; NB=Nordkapp Basin; NBB=North Barents Basin; OB=Olga Basin; PH=Polarrev High; PSB=Pechora Sea Basin; SB=Sørkapp Basin; SBB=South Barents Basin; SH=Sentralbanken High; SS=Shtokman Saddle; STH=Stappen High; TB=Tromsø Basin; and TPB=Timan-Pechora Basin. A detailed description of the structural elements can be found in Gabrielsen et al. (1990).

the 1970s with the first wells drilled in the 1980s. Nearly all drilling was done in south-southwestern areas of the shelf, whereas the northern NBSS sector (north of 74°30') has not yet been opened to exploration; thus, lithologic and stratigraphic information from this sector is currently restricted to the published literature and shallow boreholes (Figure 1B). On the Russian part of the shelf (eastern BSS, RBSS; Figure 1B), most drilling has taken place in the southeast, where correlations with nearby wells from the better-known Timan-Pechora Basin (Figures 1B, C) have been attempted (e.g., Johansen et al., 1993; Mørk, 1999).

The Upper Triassic–Lower Jurassic BSS succession is a hydrocarbon-rich interval (Polyakova, 2015), which has been tectonostratigraphically related to evolution of the Novaya Zemlya orogeny (Figure 1) bounding the BSS margin to the east (e.g., Bergan and Knarud, 1993; Olaussen et al., 2018; Martins et al., 2022). It has been suggested that far-field tectonism related to this orogeny triggered processes such as structural reactivation and salt mobilization (e.g., Indrevær et al., 2017; Hassaan et al., 2020; Martins et al., 2023), though regional ties to Novaya Zemlya tectonism are still under debate (e.g., Olaussen et al., 2018; Müller et al., 2019; Gilmullina et al., 2021). Among various analytical methods used to address this issue (e.g., Olaussen et al., 2018; Zhang et al., 2018), detailed flexural analysis (e.g., Karner and Watts, 1983; Quinlan and Beaumont, 1984; Ettensohn, 1985) remains underused but is

essential because the development of the Novaya Zemlya orogen implies BSS crustal loading, flexural responses, and related far-field tectonics. Use of flexural analysis can greatly resolve complex geologic problems ranging from tectonics (Karner and Watts, 1983) to stratigraphy (e.g., Ettensohn et al., 2019).

To evaluate the potential likelihood of Late Triassic–Early Jurassic BSS far-field reactivation, foreland-basin development, and possible ties to Novaya Zemlya tectonic loading, the goal of this study is to see if the "tectophase" model, which is built on traditional, viscoelastic, flexural theory (Quinlan and Beaumont, 1984), can tie BSS stratigraphy to compressional tectonics in the nearby Navaya Zemlya orogen (e.g., Johnson, 1971; Barbeau, 2003; Su et al., 2009; Ettensohn et al., 2019). In this model, presence of sequence-bounding unconformities, occurrence of key lithologies, and regional variations in stratigraphic thicknesses indicate responses to flexurally related structures (e.g., foreland basins and bulges) and far-field structural reactivation across a craton (Ettensohn, 1994). Hence, if Novaya Zemlya compressional tectonism occurred during Late Triassic–Early Jurassic time, coeval BSS structural reactivation and stratigraphic responses should be expected. To achieve this goal, a systematic analysis of the BSS Upper Triassic–Lower Jurassic succession was performed using 85 wells, two shallow cores, and specialized literature (e.g., Ettensohn et al., 2019).

It is important to understand word usage involving the "tectophase" concept. The term "tectophase" was defined as being the series of compressional events occurring during an orogenic event (Johnson, 1971) from the time of cratonward thrusting to the later far-field reactivation of structures across the adjacent craton and foreland basin. In contrast, "tectophase model" is the use of traditional flexural theory (e.g., Quinlan and Beaumont, 1984) to better describe foreland lithostratigraphic composition in terms of simultaneous orogenic events (Ettensohn, 1985). Similarly, the "tectophase cycle" represents a systematic succession of specific, high-resolution, foreland-basin stratigraphic units, the repetition of which reflects repeated smaller-scale compressional pulses during a larger orogeny. This stratigraphic succession is bounded by unconformities and represents lithologic responses to specific and well-defined flexural orogenic events controlled by deformational loading in the orogen (Ettensohn et al., 2019; section 1.3). Such "tectophase" successions are better studied in the Appalachian foreland basin (Ettensohn et al., 2019). Outside the Appalachian area, tectophase sequences have been identified in South China (Su et al., 2009) and the BSS (Martins et al., 2022), and other potential tectophase successions exist in the north Alpine foreland basin (Sinclair et al., 1991; Kempf and Pfiffer, 2004). Also important in this paper is defining the term "structural reactivation," which in this paper is suggested as a means to investigate potential far-field stresses in terms of stratigraphic responses.

The tectophase model is well-known in the Appalachian foreland basin in the eastern U.S.A, and it has been largely calibrated there (e.g., Ettensohn et al., 2019). Furthermore, Appalachian tectonics and geodynamics have been suggested as analogous to processes forming the Uralian-Pai-Khoi-Novaya Zemlya system of basins, which includes the BSS (e.g., Artyushkov and Baer, 1983; Kruse and McNutt, 1988; Puchkov, 2002; 2009; Ritzmann and Faleide, 2009; Gac et al., 2013; Martins et al., 2022). In the Appalachian system, however, relationships between stratigraphy and far-field tectonics are relatively well-understood (e.g., Klein and Hsui, 1987; Merschat et al., 2007; Hatcher, 2010; Ettensohn et al., 2019), whereas interpretation of BSS tectonic and stratigraphic evolution have at times been conflicting or uncertain. For example, Müller et al. (2019) interpreted latest Triassic (Rhaetian)–earliest Jurassic (Hettangian) phases of Novaya Zemlya bulge moveout, whereas Zhang et al. (2018) emphasized an earlier Triassic (Norian) orogenic exhumation, which implies bulge moveout of at least Norian (mid-Late Triassic) age.

Because the tectophase model, as used herein, is largely based on outcrop data, tectonostratigraphic and flexural concepts developed in this model are stratigraphy dependent. In the subsurface, well logs and cores provided datasets for this analysis. Even though seismic analyses can be used to complement basin study, BSS seismic coverage is not homogenous and at times largely inaccessible (e.g., Russian BSS). However, seismically imaged Upper Triassic–Lower Jurassic BSS reflectors used to address structural and tectonostratigraphic aspects in various parts of the BSS can be found in studies like those of Henriksen et al. (2011, 2023), Stoupakova et al. (2011), Müller et al. (2019), Gilmullina et al. (2021), Suslova et al. (2021), and Lundschien et al. (2023).

1.1 Far-field tectonics and tectophase modelling

Far-field tectonics is a process associated with the propagation of crustal stresses across an intraplate domain (e.g., Cloetingh, 1988; Ziegler et al., 1995; Parizot et al., 2020). Such stresses may cause tensional or compressional reactivation of preexisting structures up to 1700 km from a collisional/subduction zone and are capable of developing rifts, basement uplifts, and pull-apart basins far into the craton (Ziegler et al., 2002; Ussami et al., 2010; Cloetingh et al., 2015; Gianni et al., 2020). These compressional stresses include large-scale, low-amplitude undulations of the crust, which can be linked through timing, stratigraphy or structural style to coeval orogeny via supracrustal or subcrustal loading (Klein, 1994; Ettensohn et al., 2002). Structural reactivation during orogeny is for the most part coeval with flexural processes adjacent to the orogen, which are reflected in foreland-basin development. Because flexural theory has been traditionally used to better understand the physical characteristics of foreland basins (e.g., Karner and Watts, 1983; Quinlan and Beaumont, 1984), it can also be used to help resolve many compressional tectonostratigraphic nuances.

Though conceptual in origin, "flexural theory" is used in this study to indicate that a given tectonic process in the orogen (e.g., deformational/tectonic loading) results in a wavelength-like, flexural response (e.g., foreland basin and bulge) of the crust that can affect regional sedimentation (e.g., Quinlan and Beaumont, 1984). These regional responses in the adjacent foreland basin can be subdivided in stages tied to "phases" of flexure triggered by compression in the orogen (Ettensohn et al., 2019). Hence, the tectophase model is used to explain the relationship between stratigraphy and crustal flexure (Johnson, 1971; Ettensohn et al., 2019). Most studies using other methods tend to present orogeny as one, long episode of compression, even though orogenies are widely accepted to occur as multiple pulses that affect different areas of the orogen at different

10.3389/feart.2023.1305893

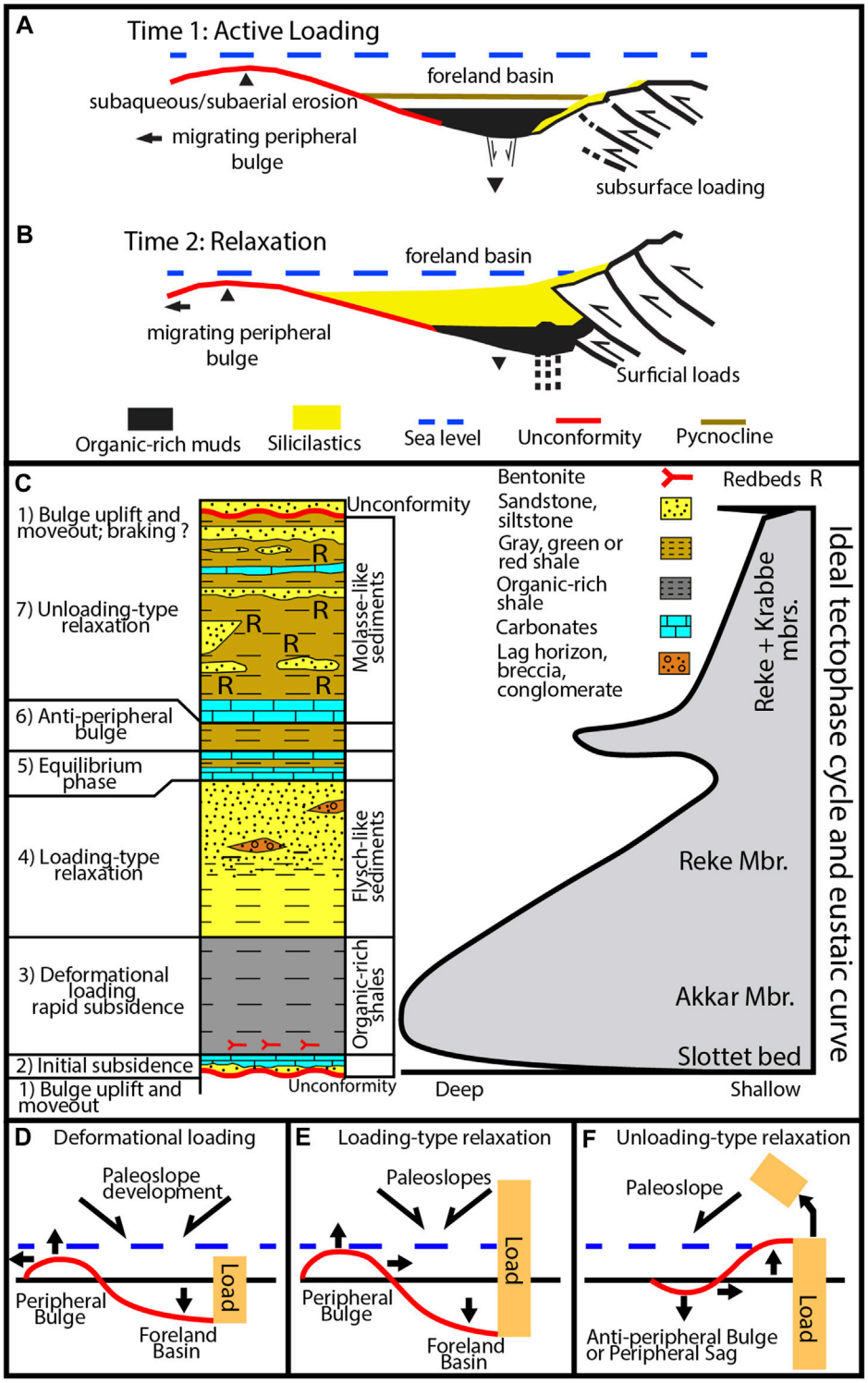

FIGURE 2
(A) and **(B)** Schematic tectonostratigraphic model illustrating deposition and structural reactivation during phases of active loading (Figure 2A) and relaxation (Figure 2B). **(C)** Schematic lithologic succession representing an ideal tectophase cycle at outcrop scale with the associated eustatic curve. Complete sequences are typically unconformity-bound and include organic-rich rocks, flysch-like sediments, and molasse-like sediments. Units under the curve on the right are representative of the Upper Triassic–Lower Jurassic NBSS succession that will be discussed later in the paper. **(D)**, **(E)**, and **(F)** Schematic flexural model illustrating phases of deformational loading, loading-type relaxation, and unloading-type relaxation (modified from Ettensohn et al., 2019).

times (e.g., Camacho et al., 2005; DiPietro, 2018). Hence, the tectophase model is useful because it can relate unconformity-bound stratigraphic sequences to smaller-order tectonic pulses in the foreland basin and adjacent intracratonic basins reactivated by coeval far-field tectonics. It is important to note, however, that the tectophase model and cycle are used as tools to provide tectonostratigraphic and flexural interpretations that tie lithostratigraphic composition to simultaneous compressional responses in the adjacent orogen. Hence, this study does not aim to provide a traditional structural analysis, as the use of seismic (e.g., Alania et al., 2018) or numerical modeling (e.g., Garcia-Castellanos et al., 1997) would do, but rather to show how the use of tectophase concepts can provide helpful and, most importantly, easy observation of far-field effects in the stratigraphy generated by compressional tectonics.

1.2 Sedimentary cyclicity in foreland basins

In most basins, sedimentary cyclicity is controlled by the interaction of tectonics, sedimentary supply, and eustacy (e.g., Miall, 1997). Understanding stratigraphic sequences as predictable patterns and cyclic responses to eustacy (sequence-stratigraphic techniques; e.g., Vail and Mitchum, 1977; Vail, 1987; Posamentier and Morris, 2000; Catuneanu et al., 2011) has become a classic method in basin analysis. This method was initially developed in extensional settings (e.g., Brown and Fisher, 1977), but their same basic concepts (e.g., retrogradation and progradation) have been used in compressional settings with some degree of success (e.g., Van Wagoner and Bertram, 1995). However, in foreland basins, flexural models (e.g., Jordan, 1981; Karner and Watts, 1983; Quinlan and Beaumont, 1984; Ettensohn, 1985; Beaumont et al., 1987; 1988; Klein and Hsui, 1987; Ziegler, 1987; Klein, 1994) are more appropriate in addressing the resulting relationships among deformational loading, depositional regime, and reactivation of basement structures by far-field forces (Ettensohn, 1987; Ettensohn, 2004; Ettensohn, 2008; Ettensohn et al., 2019).

In tectonostratigraphy, the above relationships may also be explained using tectophase cycles. Inasmuch as orogenies typically progress as a series of pulses (Johnson, 1971; Jamieson and Beaumont, 1988; DiPietro, 2018), tectonostratigraphic responses necessarily manifest as a series of unconformity-bound cycles related to each pulse of crustal loading and relaxation during a few millions to tens of millions of years (Ettensohn et al., 2019).

1.3 The tectophase cycle

Ideally, the tectophase cycle consists of a stratigraphic succession consisting of seven distinct and systematic tectonostratigraphic responses, produced as subsurface and surface thrust sheets load the lithosphere (Figure 2) (Ettensohn, 1985). Initially, to isostatically compensate for the load, the lithosphere downwarps into a flexural foreland basin with an uplifted, distal, peripheral bulge that migrates cratonward (Figure 2A). The migrating bulge typically generates a regional, sequence-bounding unconformity that defines the base of the tectophase cycle (Figures 2A, C [part 1]). As deformational loading progresses, rapid foreland-basin subsidence ensues, and the initial response is typically a thin, transgressive, shallow-water carbonate or clastic unit (Figure 2C, [part 2]). Because initial loads are mostly in the subsurface, siliciclastic influx is minor, and subsidence outpaces sedimentation. As a result, organic matter from the water column predominates in starved-basin conditions, generating dark, organic-rich muds (Figures 2A, C [part 3], D) (Ettensohn, 2008; Ettensohn et al., 2019).

As deformation continues, the load eventually becomes subaerial and drainage nets develop. One key assumption of the tectophase model is that once deformation has ceased and the load becomes static, drainage nets and erosion begin the transfer of sediment from the upland load into the adjacent foreland and outlying basins (Johnson, 1971; Ettensohn et al., 2019). However, because the load is now effectively stationary, the lithosphere relaxes in response to the static load and begins to subside while the bulge moves back towards the load (Figure 2E). This process marks the beginning of loading-type relaxation in the tectophase cycle (Figure 2B). Because of crustal relaxation and erosion (Figure 2C [part 4], E), the deepening foreland basin fills with "flysch-like" sediments that might include deeper-water deltaic, turbidites, contourites, and debris flows (Figure 2C [part 4]; 3E) (Martins et al., 2022).

Once the static surface load is eroded and the rate of sediment influx exceeds the rate of basin subsidence, the foreland basin eventually fills or overflows with sediment. At this point, a brief period of elevational equilibrium between the basin and eroded load is established, allowing the deposition of a thin blanket of shallow-water carbonates or shales across the area (Figure 2C, [part 5]). At this phase in the model, compressional tectonism ends and the stationary "equilibrium" stage represents a transition between maximum loading-type relaxation and the succeeding phase of unloading-type relaxation. This phase of equilibrium is short-lived, as parts of the former orogen and adjacent foreland basin begin to rebound in response to the lost load (Figure 2F). Rebound and a compensating "anti-peripheral bulge" result in brief episode of transgression followed by a cratonward progradation of "molasse-like" sediments, including marginal-marine, fluvial-deltaic and, alluvial sediments (Figure 2C, [parts 6 and 7]). Because this flexural stage began at near-equilibrium, sea-level conditions, a single, cratonward paleoslope becomes established (Figure 2F) (Ettensohn, 1994; Ettensohn et al., 2019; Martins et al., 2022).

A bounding unconformity at the top of the sequence (Figure 2C) typically represents a new pulse of tectonism, indicating inception of the next tectophase cycle. The above description represents an ideal depositional cycle, but parts of the succession may be poorly developed, or truncated by an overlying unconformity.

The tectophase model is most applicable to subduction-type orogenies, during which the deformational load must first mount the continental margin during early parts of the margin's convergence history (Ettensohn and Lierman, 2015; Martins et al., 2022). The thick load developed during this process piles up at the margin ramp, generating a relatively narrow, deep foreland basin in which one or more tectophase cycles (Figure 2) are deposited. However, by the time collision is imminent, the deformational load has typically surmounted the continental margin and advanced some distance across the

foreland as a surficial load. Because the load is now more expansive and spread out across the foreland, lithospheric flexure generates a broader, shallower foreland basin, in which a typical tectophase cycle will not develop. Instead, the basal unconformity is overlain by a thick sequence of marginal-marine to terrestrial clastic sediments that overflow well beyond the shallow foreland basin, generating a siliciclastic blanket that can spread hundreds of kilometers across the foreland (Ettensohn, 1994; Ettensohn, 2004; Ettensohn et al., 2019). Such a thick clastic blanket at the end of one or more tectophase cycles typically reflects a shallow, overfilled foreland basin, generated during the final, late-stage collisional orogeny at a convergent margin (Ettensohn et al., 2019).

2 Materials and methods

This study examines Upper Triassic–Lower Jurassic sections in exploration wells from the south-central NBSS (78) and RBSS (seven) (Figure 1C). Lower Jurassic parts of the section are already well-understood (e.g., Olaussen et al., 2018) and were examined largely through the literature. This study will focus on the Upper Triassic parts of the section, which are less well-understood and represented by the Fruholmen Formation in the NBSS and equivalent rocks in the RBSS.

NBSS well data for the studied sections are publicly available online from the Norwegian Petroleum Directorate (NPD, 2023), whereas RBSS well data for equivalent deposits were obtained from selected literature (Chirva et al., 1990; Astafiev et al., 2008; Gavrilov et al., 2010; Norina et al., 2014; Burguto et al., 2016; Gilmullina et al., 2021). For the NBSS, only wells that pierced the entire Fruholmen Formation were examined, whereas in the RBSS, approximately equivalent chronostratigraphic intervals were adopted from the literature. Moreover, 14 NBSS well logs were obtained from the NPD (ten are publicly available; NPD, 2023) and used for correlation (Figure 1B). Thicknesses and lithologic changes across the NBSS were measured from gamma-ray (GR), density (DE), and neutron (NP) logs. Well logs were not available for the RBSS.

Minimum and maximum thicknesses of the Fruholmen Formation (~Norian–Rhaetian) were obtained from NBSS wells, whereas equivalent thicknesses from RBSS wells are presented as obtained per individual well. For assessing these thicknesses, gamma-ray (GR), density (DE) and neutron-porosity (NP) well logs were used. The thicknesses in each well are presented as interpreted by the NPD and Russian literature and were used for regional interpretation of thickness patterns. Additionally, two northern NBSS cores from shallow stratigraphic boreholes (7934/8-U-1, and 7533/2-U-2) were provided by the NPD (Figure 1B). These cores are equivalent to lower parts of the Fruholmen Formation and were used to illustrate key stratigraphic features. Chronostratigraphy is based on the literature (e.g., Paterson and Mangerud, 2019; Gilmullina et al., 2021). For the NBSS, a west-east section was constructed and correlated with the reference well log section (Dalland et al., 1988) for the Fruholmen Formation (Figure 1B [green symbol]). The tops and bottoms of the Fruholmen Formation are noted as currently adopted by the NPD (NPD, 2023). For the RBSS, however, well logs were not available. Along this section line, key stratigraphic units (see section 3.2) were picked and correlated.

2.1 Limitations

In the tectophase model, presence and distribution of unconformable surfaces indicate inception of compressional tectonics. However, these features might also reflect sea-level variations or some combination of eustasy and tectonics, and determining which mechanism predominated is difficult (Embry, 1997). Ideally, tectophase cycles are better analyzed in present or former foreland basins, but that is not possible due to lack of access to RBSS data. However, because every orogenic system comes with onlapping intracratonic sequences that mirror those in the foreland basin (Ettensohn, 1994) and far-field responses (e.g., Ziegler, 1987), evidence from intracratonic areas may reflect developments in the foreland basin (Ettensohn and Lierman, 2015; Ettensohn et al., 2019).

It is also important to remember that seismic data were not available for this study, and that such data are not ideal for determining the lithostratigraphic composition necessary for tectophase analyses. Moreover, the chronostratigraphic analyses presented in this study are also largely based on major lithotypes and on chronologic interpretations from previous literature studies of the area. Because these earlier literature sources pose inherent chronostratigraphic limitations, this study should be scrutinized relative to future work when higher-resolution BSS chronologic data become available. Hence, this study is merely a step toward progress in future BSS foreland studies and an attempt to test the tectophase model in a challenging geologic province where access to datasets for academic research can be of great difficulty (e.g., Russian BSS).

3 Regional setting

3.1 Tectonics

Traditionally, Late Triassic–Early Jurassic BSS compressional stresses and basin development have been tied to the Uralian-Pai-Khoi-Novaya Zemlya orogeny (e.g., Petrov et al., 2008; Sobornov and Astafiev, 2017; Sobornov, 2022). This orogenic event is the final product of the diachronous collision between Baltica and Siberia during Early Carboniferous to at least Early Jurassic time (e.g., Ziegler, 1989; Gudlaugsson et al., 1998; Puchkov, 2009; Torsvik and Cocks, 2017; Martins et al., 2022; Martins et al., 2023). During at least latest Triassic–Early Jurassic time, Novaya Zemlya was thrust westward over the eastern BSS in a final collisional event, forming a west-verging, arcuate fold-and-thrust belt (e.g., Lopatin et al., 2001; Drachev et al., 2010; Scott et al., 2010; Curtis et al., 2018) (Figure 1B) and a foreland basin in the RBSS area (e.g., Faleide et al., 2017). In contrast, the NBSS area includes several rift, strike-slip, and other intracratonic basins, as well as various structural highs, which may have been reactivated coevally due to Novaya Zemlya deformation and resulting far-field forces (e.g., Faleide et al., 2017; Indrevær et al., 2017; Martins et al., 2023).

In the eastern RBSS area, Novaya Zemlya compressional events may have started as early as Late Permian (Filatova and Khain, 2010) or Middle Triassic time (Otto and Bailey, 1995; Nikishin et al., 2011; Norina et al., 2014). The following ages have been suggested as representing Novaya Zemlya orogenic events: 1) 256 Ma and 244 Ma (Filatova and Khain, 2010; Ar-Ar); 2) 220–210 Ma

FIGURE 3
Stratigraphic compilation and interpreted depositional environments from selected BSS locations (Figure 1; black line and numbers) and adjacent areas. Key references include Dalland et al. (1988); Mørk et al. (1989); Mørk (1999); Johansen et al. (1993); Grogan et al. (1999); Riis et al. (2008); Margulis (2009); Smelror et al. (2009); Stoupakova et al. (2011); Lundschien et al. (2014); Norina et al. (2014); Ryseth (2014); Spina et al. (2015); Burguto et al. (2016); Fleming et al. (2016); Lerch et al. (2016); Sobornov and Astafiev (2017); Olaussen et al. (2018); Khudoley et al. (2019); Paterson et al. (2016); Paterson and Mangerud (2017, 2019); Line et al. (2020); Gilmullina et al. (2021); and Martins et al. (2022). Formation names and ages are compiled from Dibner and Krylova (1963); Embry (1992); Mørk (1999); Schenk (2011); Lord et al. (2014); Paterson and Mangerud (2017, Paterson and Mangerud (2019); Line et al. (2020); and Gilmullina et al. (2021).

(Zhang et al., 2018; Apatite Fission Track); and 3) 210–196 Ma (Korago et al., 1992; K-Ar). In the western NBSS area, however, North Atlantic extensional events were also a tectonic force that may have begun as early as latest Devonian–earliest Carboniferous time (Stemmerik, 2000).

3.2 Structural development

A simplified framework for this complex structural zone is presented in Figure 1B, which is largely a product of the Timanian (Late Proterozoic–Early Cambrian) and Caledonian orogenies (Early Paleozoic) (Drachev, 2016). These basement structures have been repeatedly reactivated by compressional tectonics and far-field stresses triggered by at least the Timanian, Caledonian, and Uralian-Pai-Khoi-Novaya Zemlya (Late Paleozoic–Middle Mesozoic) orogenies (Nikishin et al., 1996; Petrov et al., 2008; Drachev, 2016; Smelror and Petrov, 2018; Klitzke et al., 2019). Addressing the Timanian, Caledonian, and pre-Novaya Zemlya orogenies is beyond the scope of the study, but detailed descriptions of these tectonic events can be found in McKerrow et al. (2000), Roberts and Siedlecka (2002), and Puchkov (2009). During the Novaya Zemlya phase of the Uralian orogeny, a period of intense reactivation of basement structures was triggered across the entire BSS (Anell et al., 2013; Müller et al., 2019).

3.3 Stratigraphy

During Triassic time, deltaic progradation, mostly derived from the southeast, generated widespread offshore-marine and fluvio-deltaic sedimentation across most of the BSS (e.g., Glørstad-Clark et al., 2010; Uchman et al., 2016; Gilmullina et al., 2021). Even though this pattern of sedimentation was largely maintained throughout Late Triassic time (e.g., Fleming et al., 2016) (Figure 3), progradation from the east gradually became

preeminent (Klausen et al., 2016; Khudoley et al., 2019). During Late Triassic time, widespread fluvio-deltaic deposition restricted open-marine sedimentation to northern BSS areas (Figure 3, columns 3, 5, 8, 9, 11, 12, 16) (Riis et al., 2008; Klausen et al., 2015; 2019; Sømme et al., 2018).

Across the NBSS and Svalbard (Figure 1), Upper Triassic marginal-marine to fluvio-deltaic sediments (Snadd Fm., Carnian; Figure 3, columns 1–4, 7–10, 13–18) include sandstones and interbedded mudstones overlain by coal-bearing, coastal-plain sediments and fluvial red beds (Smelror et al., 2009; Lundschien et al., 2014; Olaussen et al., 2018). In the RBSS (Figure 3, columns 5, 6, 11, 12, 19–21), equivalent deposits include an alternation of dark-gray mudstones, clayey, dark-gray siltstones, fine-to medium-grained sandstones, and coal (Gavrilov et al., 2010; Shkarubo et al., 2017). During Early Norian time, the Pan-Arctic transgression pushed the shoreline to the southern and eastern borders of the South Barents Basin (Figure 1), which remained a "sediment sink" for the nearby delta (Dalland et al., 1988; Johansen et al., 1993; Embry, 1997; Klausen et al., 2015; Burguto et al., 2016; Shkarubo et al., 2017; Olaussen et al., 2018) (Figure 3). A sharp shift from the deposition of immature, largely Carnian arkosic sands (Snadd Fm.) to mature, orthoquartzitic sands in the overlying Fruholmen Formation was coeval with this transgression (Bergan and Knarud, 1993; Ryseth, 2014), and the resulting surface of transgression may reflect a combination of several smaller erosional events and/or ravinement surfaces (Figure 3).

During Norian time across the NBSS, fluvio-deltaic sedimentation was replaced by dark, open-marine shales (Akkar Mbr.; Figure 3, columns 4, 7–9, 13, 15–18), which grade upward into interbedded coastal to fluvial sandstones (Reke Mbr.; Norian–Rhaetian) and interfingering marine shales and delta-plain sandstones (Krabbe Mbr.; Rhaetian); these three members (Akkar, Reke, and Krabbe) constitute the Fruholmen Formation (Figure 3) (e.g., Mørk et al., 1999; Paterson and Mangerud, 2019). On eastern Svalbard, Hopen Island, Kong Karls Land, and Kong Karls Platform, the Fruholmen-equivalent Flatsalen Formation includes a prominent, basal, glauconitic, carbonate bed (Slottet Bed; Figure 3, columns 1–4) which is comparable with the basal Fruholmen Formation (Lord et al., 2014; Olaussen et al., 2018). This bed is overlain by dark mudstones, followed by shallow-marine to fluvial sediments, which interfinger with marine shales (Klausen et al., 2014; Lord et al., 2014; Paterson and Mangerud, 2017). The Fruholmen and Flatsalen formations are overlain by uppermost Triassic–Lower Jurassic sandstones with subordinate shales and coals of the Tubåen (Figure 3, columns 4, 8–10, 13, 14, 16, 18) and Svenskøya (Figures 1, 3) formations, though these deposits are eroded at some locations (Dalland et al., 1988; Lord et al., 2014; 2019; Paterson and Mangerud, 2019).

Across the RBSS (Figures 1, 3; columns 5, 6, 11, 12, 19–21), official stratigraphic nomenclature has not yet been defined. However, deposits comparable to the Fruholmen Formation generally consist of alternations of interbedded, black-to-brown mudstones, siltstones, and sandstones (Burguto et al., 2016; Shkarubo et al., 2017). These Upper Triassic deposits are correlative with the Korothaikhinskaya Formation in the Korothaika Basin and with the Nar'yanmarskaya Formation in the Timan-Pechora Basin (Figures 1, 3), respectively, whereas the Lower Jurassic section is eroded (Mørk, 1999; Gilmullina et al., 2021). In Franz Josef Land (Figure 1), the target succession is defined as the Vilchekovskaya (very fine to fine sandstones with thin interbeds of shale and siltstone), Vasilevskaya (pebbly sandstones interbedded with shale, siltstone, and coal) and Tegetkhoffskaya (medium-grained sandstones with few interbeds of siltstone, shale, and coal) formations (Dibner and Krylova, 1963; Embry, 1992; Ershova et al., 2022) (Figure 3). By at least latest Triassic (Rhaetian) time, a regional unconformity was generated (Figure 3), superimposed by shallow-marine to fluvial-deltaic clastics (Dalland et al., 1988; Smelror et al., 2009; Line et al., 2020). In seismic, however, the bounding Rhaetian unconformity has angular relationships with underlying reflectors (e.g., Astafiev et al., 2008; Smelror et al., 2009; Drachev, 2016; Müller et al., 2019).

4 Results

During orogenesis, structures may reactivate with different intensity, among other factors (e.g., rheology), depending on the orientation of each structure to orogenic stresses. Availability of space for sediment accumulation will be controlled by these far-field processes and reflected in sedimentary thicknesses and facies. Moreover, the kinematic nature of each structural response to reactivation will invariably influence accumulation at local scales. In the tectophase model (Figure 2), occurrence and distribution of basal black shales and underlying unconformities clearly reflect the far-field effects of orogeny (Ettensohn and Lierman, 2015). Even though black shales and unconformities represent important stratigraphic evidence for structural reactivation, the distribution of overlying clastic wedges can also be important (Ettensohn, 2004). To evaluate far-field effects across the BSS, this study examines the following criteria: 1) the spatial variations in Norian–Rhaetian sedimentary thickness; 2) possible far-field responses from local structures; 3) unconformities; and 4) evidence of a pre-Rhaetian (mid-Late Triassic) orogenic pulse.

4.1 Thickness variations

The lithostratigraphic characteristics (e.g., composition) and thicknesses of BSS Norian–Rhaetian sediments were compiled from the 85 wells shown in Figure 1C. In the RBSS, only seven wells were available (Figure 1C; Table 1), and the thicknesses are typically presented in terms of grouped time intervals that were interpreted to represent Norian–Rhaetian thicknesses. However, a few of these reflect incomplete sections (Table 1), which may be the consequence of post-depositional erosion (Figure 3). In these RBSS wells, the recovered succession is thickest (~730 m) in the Ludlovskaya Saddle and thinnest in the west Kola Saddle (~57 m) (Figure 1B; Table 1).

In the NBSS, thickness values for the available 78 wells are shown individually per structural element (Figure 1C; Figure 4). The NBSS Norian–Rhaetian succession (Fruholmen Formation) is thickest (~580 m) near the Bjørnøyrenna Fault Complex (BFC; Figures 1, 4) and thinnest in platform areas (~15 m) (FP and BP; Figures 1, 4). The Norian–Rhaetian thicknesses for all 86 wells were then plotted in Figure 5, where five regional thickness trends are presented: 1) increased thicknesses in the central RBSS (>~300 m); 2) moderate

TABLE 1 Thicknesses for RBSS Upper Triassic sedimentary units approximately equivalent to the NBSS lower Norian–Rhaetian Fruholmen Formation (Figures 1, 3).

Well	Location	Thickness (m)	Target interval
Ludlovskaya-1	Ludlovskaya Saddle	730	Norian–Rhaetian
Severo-Kildinskaya-80	west Kola Saddle	57	Norian
Arkticheskaya-1	South Barents Basin	498	Norian–Rhaetian
Shtockmanovskaya-1	South Barents Basin	299	Norian–Rhaetian
Fersmanovskaya-1	Fersmanovskaya High area	198	Norian–Rhaetian
Severo-Murmanskaya-1	South Barents Basin	212	Rhaetian
Krestovaya-1	Admiralty High	178	Norian–Rhaetian

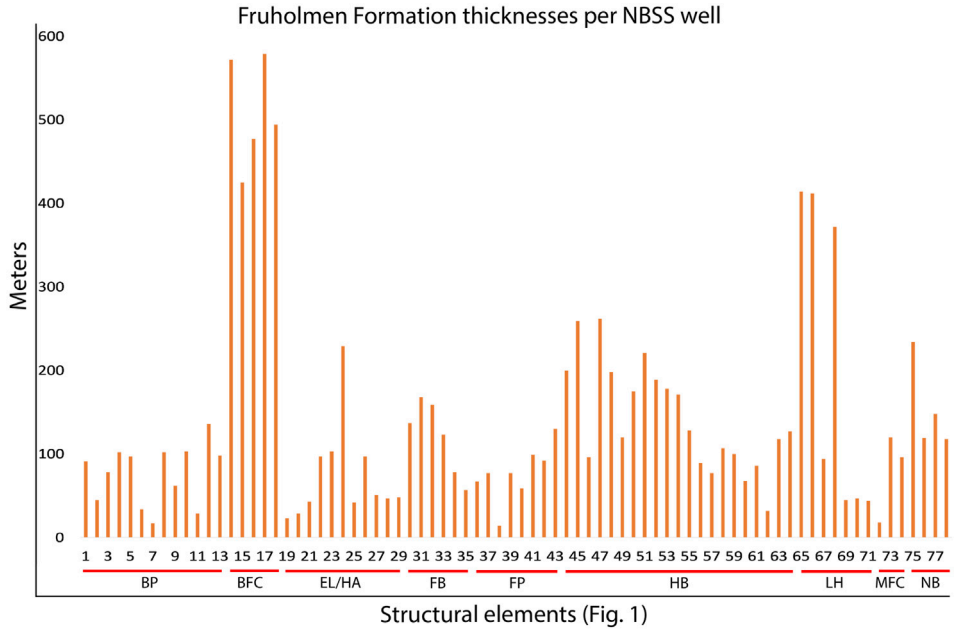

FIGURE 4
Thickness values for the Fruholmen Formation in 78 NBSS wells (Figure 1B) relative to structural elements (Figure 1A). BP=Bjarmeland Platform; BFC= Bjørnøyrenna Fault Complex; EL/HA=East Loppa/Hoop area; FB= Fingerdjupet Basin; FP=Finnmark Platform; HB=Hammerfest Basin; LH=Loppa High; MFC= Måsøy Fault Complex; and NB=Nordkapp Basin. See Figure 1B for location of structural elements and Figure 1C for approximate locations of the wells. A detailed description of the structural elements can be found in Gabrielsen et al. (1990).

thickness in the southernmost RBSS (~130–250 m); 3) thin to moderate thicknesses in the central BSS area (~15–140 m); 4) thin to moderate thicknesses in the central NBSS area (~20–230 m); and 5) increased thickness in the westernmost NBSS area (~400 m). Of these 78 wells, maximum and minimum thicknesses for the Fruholmen Formation per NBSS structural element are shown in Table 2.

4.2 Well-log succession analysis

Use of available NBSS well logs resulted in the construction of a largely west-east section line. For the RBSS, well logs were not available. Along this section line, the tops and bottoms of the Akkar (purple), Reke (yellow) and Krabbe (green) members of the Fruholmen Formation were picked and correlated (Figures 3, 6). The Akkar Member represents a predominantly deep-marine succession with abundant organic-rich muds on top of glauconitic carbonate beds and underlying fluvio-deltaic sediments (Snadd Formation; Figure 3). The Reke Member includes interbedded, shallow-marine to fluvial deposits, whereas the Krabbe Member represents an intercalation of marine and fluvio-deltaic sediments (Figure 3). In the wireline logs (Figure 6) the Akkar Member is characterized by high gamma-ray responses and simultaneous separation between density and neutron curves, whereas the Reke Member is represented by lower gamma-ray responses and minor separation of the density and neutron curves. The Krabbe Member exhibits oscillating, low-to-high, gamma-ray responses and separation of the density and neutron curves Table 3.

In the section, the Fruholmen Formation is thicker in the Hammerfest (well 7120/12-1; 198 m) and Nordkapp (well

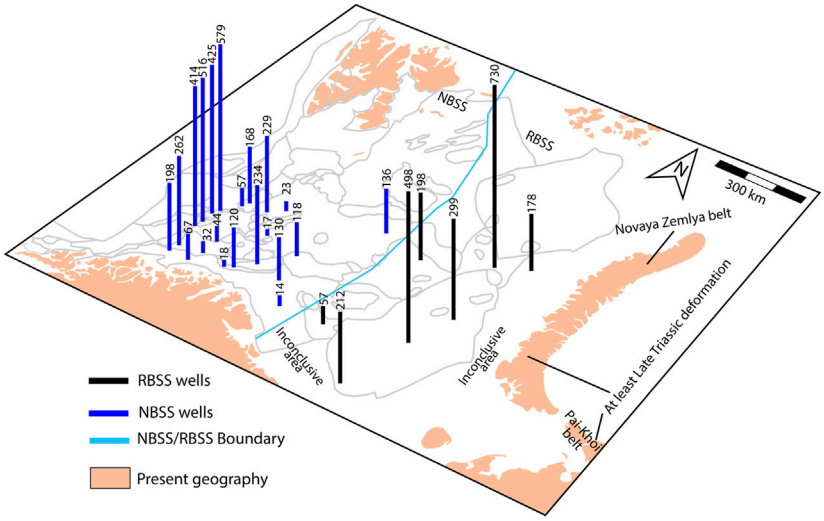

FIGURE 5
Maximum and minimum thicknesses for the Fruholmen Formation on the NBSS (blue) and maximum thicknesses for approximately equivalent deposits on the RBSS (black). The positions of the columns represent the approximate well locations (see Figure 1C).

TABLE 2 Maximum and minimum Fruholmen Formation thicknesses across selected NBSS structural elements (Figure 1).

Well	Location	Thickness (m)	Well	Location	Thickness (m)
7225/3-2	Bjarmeland Platform	17	7132/2-2	eastern Finnmark Platform	14
7335/3-1	Bjarmeland Platform	136	7229/11-1	eastern Finnmark Platform	130
7220/2-1	Bjørnøyrenna Fault Complex	425	7122/7–7 S	Hammerfest Basin	32
7220/7–2 S	Bjørnøyrenna Fault Complex	579	7120/9-2	Hammerfest Basin	262
7324/2-1	eastern Loppa High	23	7222/11-2	Loppa High	44
7324/7–3 S	eastern Loppa High	229	7120/1-1	Loppa High	414
7321/8–2 S	Fingerdjupet Basin	57	7124/4–1 S	Måsøy Fault Complex	18
7321/7-1	Fingerdjupet Basin	168	7125/4-1	Måsøy Fault Complex	120
7122/10–1 S	western Finnmark Platform	67	7228/7–1 S	Nordkapp Basin	118
7120/12-1	western Finnmark Platform	198	7227/10-1	Nordkapp Basin	234

7227/10-1; 234 m) basins (Figure 6), but thinner on the Loppa High (well 7222/11-1; 47 m). All three members of the Fruholmen Formation are distinguishable in the well logs, except in well 7222/11-1 (Loppa High; Figure 1), where the Krabbe Member (Figure 6; green) is absent. Clearly, all members show variations in thickness from well to well (Figures 1, 6), but more important are the larger-scale changes in thickness patterns as the section progresses from west to east across various structures. In the four western wells, for example, the entire section is thicker and probably reflects deposition in a basinal setting. The section then dramatically thins in well 7222/11-1 as it moves across the Loppa High, but again thickens moderately on the intervening Bjarmeland Platform. This thickness trend is maintained eastwardly until the Nordkapp Basin (well 7227/10-1; 234 m), where the section again thickens abruptly. South and east of this well, including the southern edges of the basin and adjacent platform areas (Finnmark Platform), thicknesses again become moderate (e.g., Figure 6; ~130 m). It is important to note that the three different members commonly vary in thicknesses independently of each other (Krabbe Mbr., Figure 6).

Of the three members, the Akkar Member is probably the most important because variation in accommodation space for these shales represents regional processes associated with the beginning of deformational loading as reflected in the tectophase succession (Figure 2). The thicknesses of the Akkar Member and the sum of the thicknesses of the Reke and Krabbe members are illustrated in a west-to-east graphic format (Figure 7). In Figure 7, thicknesses of the Akkar Member are highly variable, ranging from ~10 m (Well 7132/2-2, eastern Finnmark Platform; Figure 1) to 60 m (Well 7228/2–1 S, Nordkapp Basin; Figure 1), but having an average thickness of approximately 40 m (blue line; Figure 7). The graphic presentation in Figure 7 is important because it better illustrates that thickness

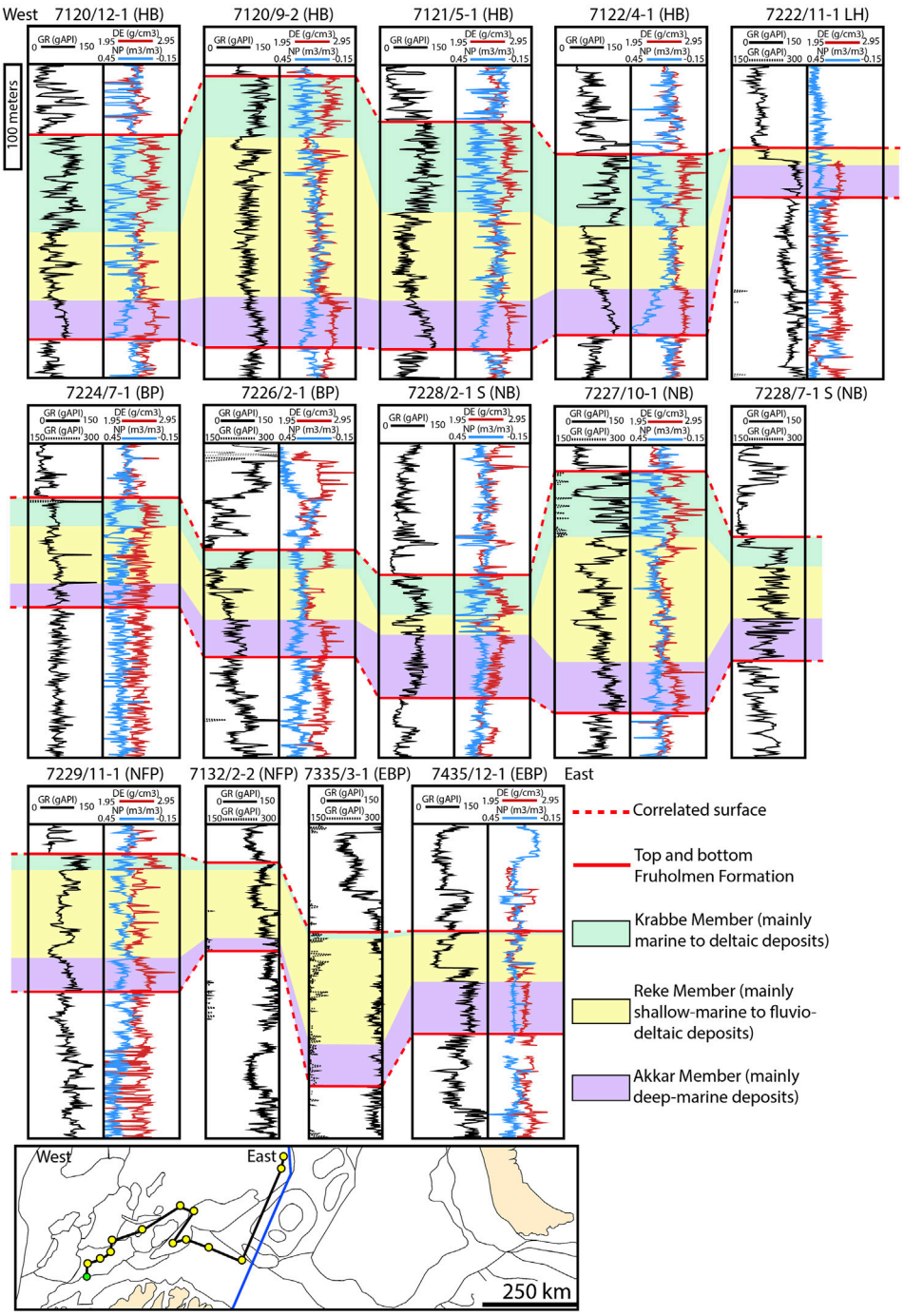

FIGURE 6
NBSS wireline-log correlation (Figure 1; Table 3). The purple, yellow and green bands represent log responses of the Akkar, Reke and Krabbe members, respectively. Well 7120/12-1 is the Fruholmen reference well used for correlation. HB=Hammerfest Basin; LH=Loppa High; BP=Bjarmeland Platform; NB=Nordkapp Basin; NFP= northern Finnmark Plaftform; and EBP=eastern Bjarmeland Platform.

variations in the basal Akkar Member are apparent from the beginning of sequence deposition.

4.3 Unconformities

In the tectophase model, presence and distribution of unconformable surfaces are important because these features commonly reflect flexural, bulge-moveout responses to the inception of orogeny (Figure 2). Within the Upper Triassic–Lower Jurassic BSS succession, two such surfaces are present. The youngest surface (Rhaetian–Hettangian) (Figure 3) has been traditionally interpreted as an unconformity because of its prominent seismic angularity and regional distribution (e.g., Astafiev et al., 2008; Drachev, 2016; Müller et al., 2019). In the shallow core 7533/2-U-2 (Figure 8A), this surface reflects subtle

TABLE 3 Selected wireline logs used to compose the NBSS stratigraphic and correlation section (Figure 1).

Well	Location	Well	Location
7120/12-1	Hammerfest Basin	7228/2–1 S	Nordkapp Basin
7120/9-2	Hammerfest Basin	7227/10-1	Nordkapp Basin
7121/5-1	Hammerfest Basin	7228/7–1 S	Nordkapp Basin
7122/4-1	Hammerfest Basin	7229/11-1	northeastern Finnmark Platform
7222/11-1	Loppa High	7132/2-2	northeastern Finnmark Platform
7224/7-1	Bjarmeland Platform	7335/3-1	eastern Bjarmeland Platform
7226/2-1	Bjarmeland Platform	7435/12-1	eastern Bjarmeland Platform

erosional truncation of low-angle cross stratification and was interpreted by Lord et al. (2019) to represent subaerial exposure and fluvial erosion. Below this surface, deposits are sand-rich and show hummocky-like to low-angle cross stratification (Figure 8A). Along the truncation surface, brown-colored weathering and sediments containing shale chips and siderite nodules represent a basal lag (Lord et al., 2019). Overlying grey sandstones showing wavy-like bedding that shifts to parallel low-angle cross stratification may represent a progressive decrease in energy.

Presence of a second, older unconformable surface (Early Norian; Figure 3) (e.g., Riis et al., 2008) is less clear. In the shallow core 7533/2-U-2 (Figure 8B), this Early Norian surface separates cross-bedded grey sandstones and grey to dark-grey mudstones from a prominent carbonate-rich lag horizon. The contact between this carbonate lag and underlying siliciclastic sediments is abrupt and shows evidence of scouring. In the shallow core 7934/8-U-1 (Figure 8C), however, the erosional nature of this surface is less clear, though the facies shift is abrupt. In contrast, the contact between the carbonate lag overlying organic-rich shales (Akkar Member equivalent; Figure 3) does not show significant indication of erosion in the shallow core (Figure 8D), but the color and homogeneity of the shales suggest deposition during an apparent transgressive event.

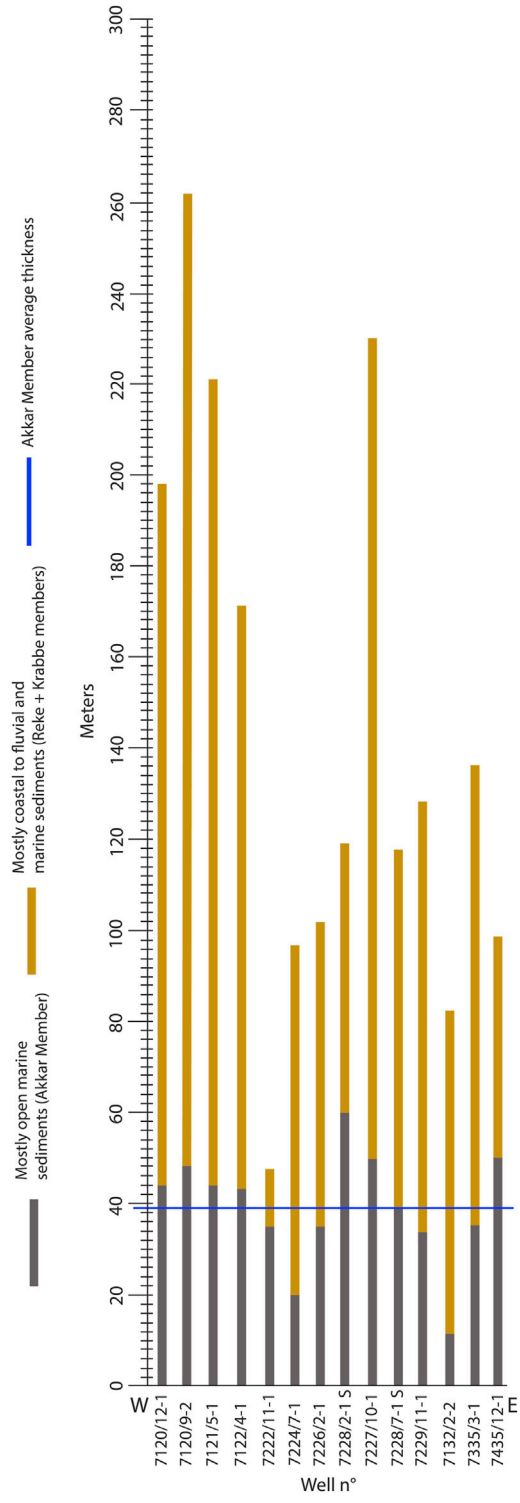

FIGURE 7
Thicknesses for the Akkar Member (dark gray) and Reke plus Krabbe members (brown) in the various wireline logs used in the correlation line (Figures 1, 6; Table 3). W = west and E = east. For well location, refer back to Figure 6.

5 Discussion

In this section, focus is placed on evidence for structural reactivation and foreland-basin development. Moreover, the target stratigraphic succession (Figure 3) and arguments from the literature are used to suggest the occurrence of two episodes of deformational loading in Novaya Zemlya during Late Triassic–Early Jurassic time.

5.1 Evidence for structural reactivation

Traditionally, the Fruholmen Formation and equivalent deposits are associated with the Early Norian Pan-Arctic transgression, which reflects a major sea-level rise along the proto-Atlantic seaway that transgressed the BSS from west to east (e.g., Johansen et al., 1993; Worsley, 2008; Olaussen et al., 2018). Assuming tectonic quiescence at the time, the simplest outcome was

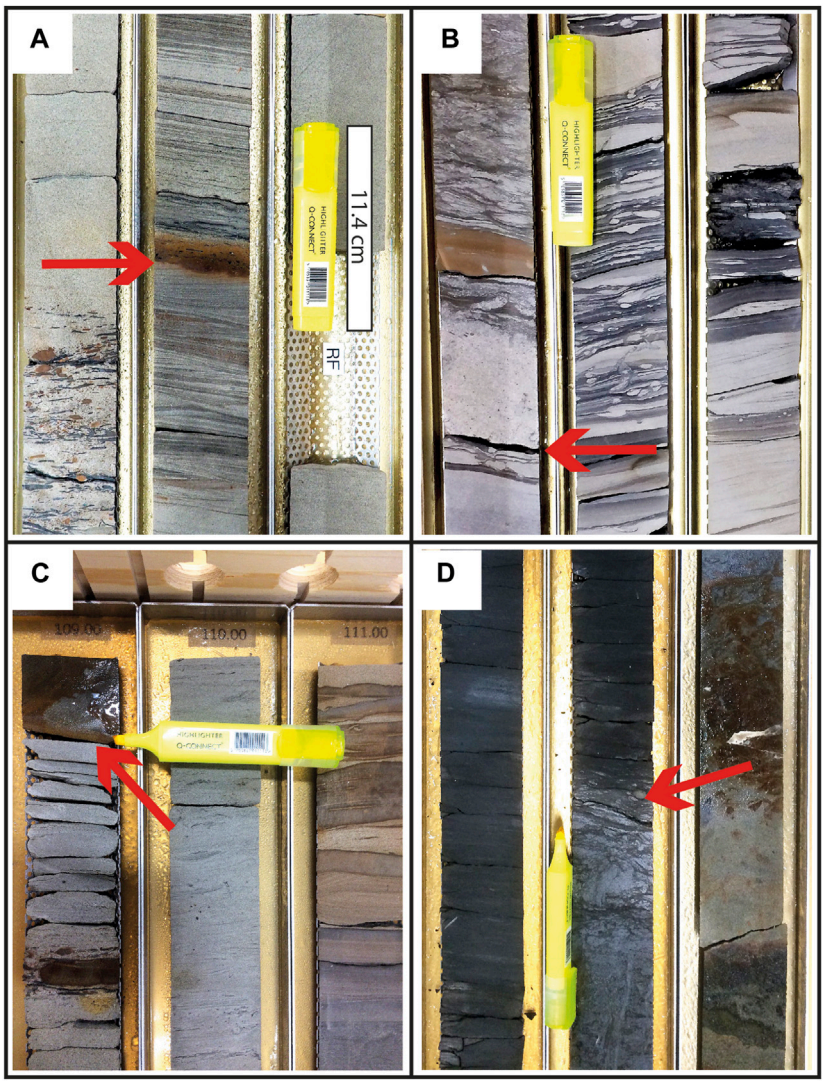

FIGURE 8
Photographs of cores from shallow boreholes 7533/2-U-2 and 7934/8-U-1 (Figure 1). **(A)** Rhaetian-Hettangian unconformity (7533/2-U-2; red arrow); **(B)** Contact between the Slottet Bed and De Geerdalen Formation (7533/2-U-2; red arrow); **(C)** Contact between the Slottet Bed and De Geerdalen Formation (7934/8-U-1; red arrow); and **(D)** Transition between the Slottet Bed and organic-rich shales equivalent to the Akkar Member (7934/8-U-1; red arrow). See Figure 1 for location and Figure 3 for formal stratigraphy. The Rhaetian unconformity in Figure 8A is from Lord et al. (2019).

for thicker deposits to occur in the western BSS, whereas the eastern BSS basins would have already been filled by the fluvial-deltaic sediments of the developing Uralide clastic wedge.

As observed in the well logs (Figure 6) and the thickness plot (Figure 7), however, Fruholmen sediments are at times thicker in eastern NBSS structures than in western areas (Figure 6). Similarly, erosion of top-Fruholmen deposits is also variable across the shelf (Figures 6, 7). It is feasible to interpret these patterns as a result of differential subsidence and uplift of BSS structures triggered by far-field structural reactivation, which suggests that structures were being simultaneously reactivated at different places across the BSS. During Late Triassic–Early Jurassic time, the Novaya Zemlya orogeny is the best candidate for triggering widespread structural reactivation across the BSS. Variations in sedimentary thicknesses of a formation deposited across different structural elements coeval with orogeny suggests episodes of structural reactivation by far-field tectonics (e.g., Ettensohn et al., 2019). This interpretation aligns well with other studies, such as those of Faleide et al. (2017), Müller et al. (2019), Müller et al. (2022), and Gilmullina et al. (2021).

5.2 Evidence for foreland-basin development

In the BSS, the North and South Barents basins (Figure 1, SBB, NBB) have been interpreted to represent a Jurassic foreland basin, formed in response to coeval Novaya Zemlya compressional tectonism (e.g., Faleide et al., 2017; Olaussen et al., 2018). Moreover, others have interpreted the orogenic exhumation of Novaya Zemlya to have occurred as early as Norian time (e.g., Klausen et al., 2016; Zhang et al., 2018), suggesting Norian tectonism with uplift and deformation. Because foreland-basin development is

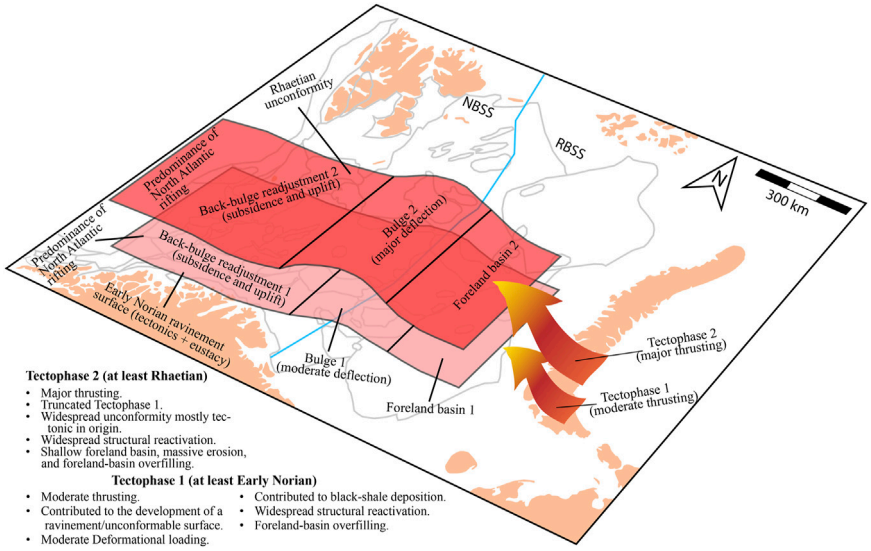

FIGURE 9
Integrative BSS map schematically illustrating the depozones associated with the two Novaya Zemlya tectophases interpreted in this paper. Tectophase 1 (at least Early Norian) represents a moderate thrusting episode, whereas Tectophase 2 (latest Rhaetian) represents a major collisional episode of thrusting. The resultant time-equivalent deposits corresponding to each tectophase is illustrated in Figure 3.

a flexural response to the inception of orogenic uplift and crustal thickening (Quinlan and Beaumont, 1984), presence of a Jurassic foreland basin implies a Jurassic pulse of orogeny, which, across the BSS, apparently occurred as early as Norian time.

Existence of two Novaya Zemlya episodes of loading and foreland-basin development integrates previous interpretations, including the presence of tectonism around the Carnian–Norian boundary (Bergan and Knarud, 1993; Embry, 1997; Fleming et al., 2016) and its culmination by late Norian time (220–210 Ma) (Zhang et al., 2018), followed by latest Triassic (Rhaetian)–earliest Jurassic tectonism, reflected in bulge and foreland-basin development (Faleide et al., 2017; Müller et al., 2019). Hence, if Upper Triassic–lowest Jurassic BSS deposits indeed represent deposition during two episodes of structural reactivation triggered by the Novaya Zemlya orogeny, then these two orogenic pulses must reflect two distinct tectophases (phases of deformational loading in the Novaya Zemlya orogen).

5.3 Tectophase sequences

Understanding the BSS Upper Triassic–Lower Jurassic succession in terms of sedimentary thicknesses, unconformity-bound sedimentary sequences, and structural reactivation leads to the presumption of multiple deformational pulses in the Novaya Zemlya orogen. Based on the work of Johnson (1971) and Ettensohn et al. (2019), multiple orogenic pulses and resultant tectophase cycles are common in many orogenic systems. Based on stratigraphic analysis, BSS sedimentary thicknesses and unconformities, two foreland-basin tectophase cycles, reflecting two Novaya Zemlya orogenic pulses during Late Triassic–Early Jurassic time (Figure 9) are suggested in the present work. In particular, the occurrence of unconformities associated with collisional systems is important because these features can reflect orogenic control beyond the foreland basin into adjacent cratonic areas (Ettensohn, 1994).

Presence of an Early Norian unconformable surface (Figure 3) has been questioned by some (e.g., Lundschien et al., 2014; Müller et al., 2019; Gilmullina et al., 2021), while other studies have interpreted it to represent a major unconformity (Figure 3) (e.g., Embry, 1997; Bugge et al., 2002; Riis et al., 2008; Ryseth, 2014; Lord et al., 2019; Olaussen et al., 2022). Moreover, some authors have interpreted this Early Norian surface to represent a sequence boundary (Riis et al., 2008; Lord et al., 2019; Rismyhr et al., 2019), whereas others have not (Paterson and Mangerud, 2019; Gilmullina et al., 2021; Klausen et al., 2022). According to Lord et al. (2019) and Olaussen et al. (2022), the lower boundary of the Slottet Bed (Figures 3, 8B) represents this Early Norian regional subaerial unconformity. In the southern NBSS, Ryseth (2014) correlated this same surface in well logs from the Hammerfest Basin (Figure 1) to at least 250 km northeast of the basin. On Svalbard outcrops, Müller et al. (2019) indicated an Early Norian unconformable horizon between the De Geerdalen and Flatsalen formations (Figure 3). In the northern BSS, Olaussen et al. (2018) noted that a similar surface is a prominent seismic horizon, and characteristics typical of an unconformity have also been suggested in the southern BSS (Bugge et al., 2002).

In this paper, we suggest the presence of an Early Norian unconformity (Lord et al., 2019; Figure 8B), which represents a subtle inception of the first tectophase, whereas the Rhaetian unconformity (Drachev, 2016; Figure 8A) represents the second unconformity (Figure 9). This interpretation does not preclude the possibility of pre-Late Triassic Novaya Zemlya orogenic episodes (Filatova and Khain, 2010; Blakey, 2021), which are beyond the scope of this study. In following sections, we define the two orogenic episodes of deformational loading triggered by tectonics in the Novaya Zemlya orogen in terms of tectophases.

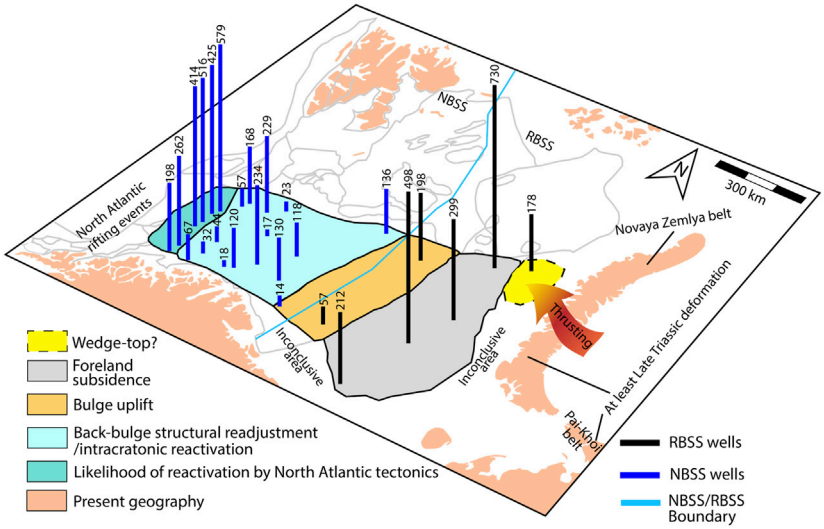

FIGURE 10
Norian–Rhaetian foreland-basin development and depozones across the southern BSS and adjacent areas. Maximum and minimum thicknesses (numbered columns) for the Fruholmen Formation on the NBSS (blue) and maximum thicknesses for approximately equivalent deposits on the RBSS (black). The positions of the columns represent the approximate well locations. The orange arrow represents thrusting associated with the Novaya Zemlya orogeny. Foreland depozone nomenclature is that of DeCelles and Giles (1996).

5.4 Tectophase 1 (Norian–Rhaetian)

From the Novaya Zemlya fold belt westward, a thin Norian–Rhaetian succession (~178-m thick, yellow) on the Admiralty High (Figures 1, 3) becomes a much thicker (up to ~500–730-m thick; gray) succession in the central RBSS areas. This region with thick deposits is surrounded by areas containing much thinner accumulations (~57–198 m, orange). From the orange area westward, formation thicknesses increase to ~118–229 m in the central NBSS (Figure 10, blue). Toward the western NBSS, in contrast, a very sharp increase in thicknesses up to ~580 m is present (Figure 10; dark green). Variation in these BSS thicknesses aligns well with the work of DeCelles and Giles (1996) (Figure 10), which suggests that use of thicknesses variations across a tectonically influenced shelf is one means to illustrate geometric patterns associated with the depositional zones of a classic foreland-basin system (DeCelles and Giles, 1996) (Figure 10).

When compared with the foreland-basin depozones of DeCelles and Giles (1996), the thickness patterns noted above strongly suggest the presence of a Norian–Rhaetian foreland-basin system (Figure 10). The interpreted foreland depozones include: 1) wedge-top (easternmost RBSS, yellow); 2) foredeep (central-southern RBSS area, gray); 3) bulge (RBSS/NBSS transition, orange); and 4) back-bulge (central NBSS, blue). The sharp increase in thicknesses in westernmost areas (NBSS, light blue) probably represents structural overprint by North Atlantic tensional processes, which began as early as Permo-Carboniferous time (e.g., Ziegler, 1989; Stemmerik and Worsley, 2005).

Based on the above assumptions, various stages of an initial tectophase cycle are observed in the Norian–Rhaetian succession. Stage 1 is characterized by unconformity development (Early Norian surface; Figures 2, 8B), which represents the mixed responses to subtle Novaya Zemlya compressional tectonics and eustacy. Stage 2 represents initial subsidence represented by a thin, overlying carbonate-rich unit (Slottet Bed; Figures 2, 8B), whereas Stage 3 represents rapid, regional, subsidence that facilitated widespread deposition of organic-rich shales (Akkar Member; Figures 2, 6, 8D). Stages 4 through 7 represent shallow-marine to fluvio-deltaic deposition (Reke and Krabbe members; Figures 2, 6), related to loading- and unloading-type sediments derived from the Novaya Zemlya orogen. This interpretation fits well with that of Zhang et al. (2018), who interpreted a period of Norian (220–210 Ma) orogenic exhumation.

Even though the cores and logs used to describe this tectophase cycle mostly occur beyond the limits of the RBSS foredeep, tectophase sequences may onlap intracratonic areas, thus providing evidence of foredeep events (Ettensohn, 1994; Ettensohn et al., 2002; Ettensohn et al., 2019). Such an onlap has been indicated by Klausen et al. (2016), who suggested that Novaya Zemlya sediments prograded well-beyond the Norian–Rhaetian RBSS foredeep as far as the western BSS area. Across the NBSS, deposition of the above succession is the result of both widespread structural reactivation by Novaya Zemlya far-field tectonics and extensive transgression. Assessing the causes for early Norian transgression is beyond the scope of this study, but Norian tectonic influence on eustacy has been noted in adjacent Arctic basins (Embry et al., 2018).

5.5 Tectophase 2 (Rhaetian–Hettangian)

Across the BSS, the Rhaetian unconformity (Figures 3, 8A) has been confidently tied to a final episode of Novaya Zemlya tectonism and coeval foreland-basin development (e.g., Drachev, 2016; Faleide et al., 2017; Müller et al., 2019). This latest Rhaetian–Hettangian

stratigraphic feature represents the inception of Tectophase 2 (Figure 9). This event was significant because it represents the final collision of Siberia with Baltica and generated a hiatus of up to 40 million years in some areas and widespread truncation of previous deposits (Figure 3) (e.g., Paterson and Mangerud, 2019), which is easily observed in seismic data (Müller et al., 2019). This unconformity is sequence-bounding and represents the inception of the Lower Jurassic foreland-basin sequence (Faleide et al., 2017; Martins et al., 2022).

This tectophase succession, however, does not contain the basal organic-rich shales and overlying flysch-like sequence that are typical of a tectophase cycle (Figure 2). Rather, this major unconformity is succeeded by a thick accumulation of shallow-marine to terrestrial clastic sediments that blankets nearly the entire BSS under names like the Tubåen and Svenskøya formations (Figure 3) Like the final Alleghanian collisional clastic sequence in the Appalachian Basin (Ettensohn et al., 2019), this widespread blanket of clastic sediments is interpreted to represent a final collisional phase of tectonism (in this case involving Siberia and Baltica) at Novaya Zemlya along with the generation of a broad, shallow foreland basin that allowed sediments to spill out across the BSS. Even though the same flexural stages still operated in development of the foreland basin, the resultant succession and stratigraphic responses differed substantially because of the collisional nature of the orogeny, resulting in a thick sequence of mostly molasse-like sediments, overfilling a shallow foreland basin (e.g., Ettensohn et al., 2019; Martins et al., 2022). Interpretation of a shallow, Jurassic RBSS foreland basin aligns well with interpretations from the studies of Suslova (2014), Gilmullina et al. (2021), and Martins et al. (2023), who noted widespread thicknesses of clastic sediments, up to 1.2 km in thickness, in a foreland basin located in the RBSS area.

6 Conclusion

Thickness variations, presence of a typical tectophase cycle, and an Early Norian (mid-Late Triassic) unconformable boundary suggest an initial stage of Novaya Zemlya orogeny and deformational loading, which supports an earlier inception of Novaya Zemlya orogeny and deformation, which we interpret here as Tectophase 1. In latest Rhaetian (latest Triassic) time, the Tectophase 1 succession was truncated by another major unconformity with a thick overlying succession of coarse, shallow-marine to terrestrial, clastic sediments, triggered by deformation from a final collisional event, representing the collision of Siberia with Baltica. This event continued into Early Jurassic time and is identified herein as Tectophase 2. Overall, this tectonostratigraphic work aligns with other studies suggesting Late Triassic to Early Jurassic Novaya Zemlya compressional stresses and structural reactivation by far-field tectonics. The conceptual tectophase model used in this study contributes to the understanding of unconformity development, stratigraphic succession, and far-field reactivation of BSS structures in both foreland and intracratonic areas.

Data availability statement

The original contributions presented in the study are included in the article/Supplementary material, further inquiries can be directed to the corresponding author.

Author contributions

GM: Conceptualization, Data curation, Formal Analysis, Investigation, Methodology, Software, Visualization, Writing–original draft, Writing–review and editing. FE: Formal Analysis, Investigation, Methodology, Supervision, Validation, Visualization, Writing–review and editing. S-MK: Conceptualization, Funding acquisition, Investigation, Project administration, Resources, Supervision, Validation, Writing–review and editing.

Funding

The author(s) declare financial support was received for the research, authorship, and/or publication of this article. This research was funded by the Norwegian Petroleum Directorate (grant 2190). Access to shallow cores and unpublished wireline-logs was granted by the Norwegian Petroleum Directorate, without which this project would not have been possible.

Acknowledgments

We would like to thank the Norwegian Petroleum Directorate for funding this research and for providing data from wireline logs and shallow cores. We also thank the editors, four anonymous reviewers, VG, GC, and Eric Barefoot for their through reviews, which enhanced the nature of the manuscript considerably.

Conflict of interest

Author S-MK was employed by Norwegian Petroleum Directorate.

The remaining authors declare that the research was conducted in the absence of any commercial or financial relationships that could be construed as a potential conflict of interest.

Publisher's note

References

Alania, V., Enukidze, O., Glonti, N., Razmadze, A., Chabukiani, A., Giorgadze, A., et al. (2018). Structural architecture of the kura foreland fold-and-thrust belt using seismic reflection profile, Georgia. *Univers. J. Geoscience* 6, 184–190. doi:10.13189/ujg.2018.060602

Anell, I., Braathen, A., Olaussen, S., and Osmundsen, P. T. (2013). Evidence of faulting contradicts a quiescent northern Barents shelf during the Triassic. *First Break* 31, 67–76. doi:10.3997/1365-2397.2013017

Artyushkov, E. V., and Baer, M. A. (1983). Mechanism of continental crust subsidence in fold belts: the Urals, Appalachians and Scandinavian Caledonides. *Appalachians Scand. Caledonides Tectonophys.* 100, 5–42. doi:10.1016/0040-1951(83)90176-2

Astafiev, B. Y., Viskunova, K. G., Voinova, O. A., Glaznev, V. N., Zhuravlev, V. A., Zhuravlev, V. I. A., et al. (2008). *State geological map of the Russian federation (in Russian): saint petersburg, VSEGUEI, The North-Kara-Barents sea series, sheets R-37 and R-38, scale 1: 1,000,000.*

Barbeau, D. L. (2003). A flexural model for the paradox basin: implications for the tectonics of the ancestral rocky mountains. *Basin Reearch* 15, 97–115. doi:10.1046/j.1365-2117.2003.00194.x

Beaumont, C., Quinlan, G. M., and Hamilton, J. (1987). "The Alleghanian Orogeny and its relationship to the evolution of the eastern interior," in *Sedimentary basins and basin-forming mechanisms: Canadian society of petroleum geologists memoir 12*. Editors C. Beaumont and A. J. Tankard, 425–445.

Beaumont, C., Quinlan, G. M., and Hamilton, J. (1988). Orogeny and stratigraphy: numerical models of the Paleozoic in the eastern interior of North America. *Tectonics* 7, 389–416. doi:10.1029/tc007i003p00389

Bergan, M., and Knarud, R. (1993). "Apparent changes in clastic mineralogy of the Triassic–Jurassic succession, Norwegian Barents Sea: possible implications for paleodrainage and subsidence," in *Arctic geology and petroleum potential*. Editors T. O. Vorren, E. Bergsager, Ø. A. Dahl-Stamnes, E. Holter, B. Johansen, E. Lie, et al. (Amsterdam: Elsevier), 2, 363–376.

Blakey, R. (2021). Paleotectonic and paleogeographic history of the Arctic region. *Atl. Geol.* 57, 007–039. doi:10.4138/atlgeol.2021.002

Brown, L. F., and Fisher, W. L. (1977). "Seismic-stratigraphic interpretation of depositional systems: examples from Brazilian rift and pull-apart basins: section 2. Application of seismic reflection configuration to stratigraphic interpretation," in *Applications to hydrocarbon exploration*. Editor C. E. Payton (Ann Arbor: Edward Brothers), 26, 51–53. Memoir.

Bugge, T., Elvebakk, G., Fanavoll, S., Mangerud, G., Smelror, M., Weiss, H. M., et al. (2002). Shallow stratigraphic drilling applied in hydrocarbon exploration of the Nordkapp Basin, Barents Sea. *Barents Sea Mar. Petroleum Geol.* 19, 13–37. doi:10.1016/s0264-8172(01)00051-4

Burguto, A. G., Zhuravlev, V. A., Zavarzina, G. A., and Zinchenko, A. G. (2016). *State geological map of the Russian federation (in Russian): saint petersburg, VSEGUEI, The North-Kara-Barents sea series, sheets S-36 and S-37, scale 1: 1,000,000.*

Camacho, A., Lee, J. K. W., Hensen, B. J., and Braun, J. (2005). Short-lived orogenic cycles and the eclogitization of cold crust by spasmodic hot fluids. *Nature* 435, 1191–1196. doi:10.1038/nature03643

Catuneanu, O., Galloway, W. E., Kendall, C. G. St.C., Miall, A. D., Posamentier, H. W., Strasser, A., et al. (2011). Sequence stratigraphy: Methodology and nomenclature. *Newsletters Stratigr.* 44, 173–245. doi:10.1127/0078-0421/2011/0011

Chirva, S. A., Morakhovskaya, E. D., Kulikova, N. K., Fedorova, V. A., and Yakovleva, S. P. (1990). "Stratigraphy of the triassic and jurassic deposits of the Barents Sea," in *Geological structure and oil and gas potential of the Arctic islands*. Editors N. S. Oknova, V. I. Slavin, and V. M. Desyatkov (Leningrad: VNIGRI), 7, 15–30.

Cloetingh, S. (1988). "Intraplate stresses: a new element in basin analysis," in *New perspectives in basin analysis*. Editor K. L. Kleinspehn (New York: Springer-Verlag), 205–230.

Cloetingh, S., Ziegler, P. A., Beekman, F., Burov, E. B., Garcia-Castellanos, D., and Matenco, L. (2015). "Tectonic models for the evolution of sedimentary basins," in *Treatise on geophysics*. Editor G. Schubert (Amsterdam: Elsevier), 6, 513–592.

Curtis, M. L., Lopez-Mir, B., Scott, R. A., and Howard, J. P. (2018). "Early Mesozoic sinistral transpression along the Phai-Khoi-Novaya Zemlya fold–thrust belt, Russia," in *Circum-Arctic lithosphere evolution*. Editors V. Pease and B. Coakley (London: Geological Society, Special Publications), 460, 355–370.

Dalland, A., Worsley, D., and Ofstad, K. (1988). *A lithostratigraphical scheme for the Mesozoic and Cenozoic succession, offshore mid- and northern Norway*, 4. Stavanger: Norwegian Petroleum Directorate, 65.

DeCelles, P. G., and Giles, K. A. (1996). Foreland basin systems. *Basin Res.* 8, 105–123. doi:10.1046/j.1365-2117.1996.01491.x

Dibner, V. D., and Krylova, N. M. (1963). Stratigraphic position and material composition of coal measures in Franz Josef Land. *Franz Josef Land Sov. Geol.* 7, 77–89. doi:10.1080/00206816509474751

DiPietro, J. A. (2018). *Geology and landscape evolution*. Amsterdam: Elsevier, 624.

Doré, A. G., Dahlgren, T., Flowerdew, M. J., Forthun, T., Hansen, J. O., Henriksen, L. B., et al. (2022). "South-central Barents Sea composite tectono-sedimentary element," in *Sedimentary successions of the Arctic region and their hydrocarbon prospectivity*. Editors S. S. Drachev, H. Brekke, E. Henriksen, and T. Moore (London: Geological Society of London), 1–23. Memoirs. 57.

Drachev, S. S. (2016). Fold belts and sedimentary basins of the Eurasian Arctic. *Eurasian Arct. Arktos* 2, 1–30. doi:10.1007/s41063-015-0014-8

Drachev, S. S., Malyshev, N. A., and Nikishin, A. M. (2010). "Tectonic history and petroleum geology of the Russian Arctic shelves: an overview," in *Petroleum geology conferences: london*. Editors B. A. Vining and S. C. Pickering (London, United Kingdom: Geological Society of London), 591–619.

Duran, E. R., di Primio, R., Anka, Z., Stoddart, D., and Horsfield, B. (2013). Petroleum system analysis of the Hammerfest Basin (southwestern Barents Sea): comparison of basin modelling and geochemical data. *Org. Geochem.* 63, 105–121. doi:10.1016/j.orggeochem.2013.07.011

Embry, A. (1997). Global sequence boundaries of the Triassic and their identification in the Western Canada sedimentary basin. *Bull. Can. Petroleum Geol.* 45, 415–433. doi:10.35767/gscpgbull.45.4.415

Embry, A., Beauchamp, B., Dewing, K., and Dixon, J. (2018). "Episodic tectonics in the phanerozoic succession of the Canadian high arctic and the 10-million-year flood," in *Circum-Arctic structural events: tectonic evolution of the Arctic margins and trans-Arctic links with adjacent orogens: boulder*. Editors K. Piepjohn, J. V. Strauss, L. Reinhardt, and W. C. McClelland (Geological Society of America), 213–230.

Embry, A. F. (1992). "Mesozoic stratigraphy of Franz Josef Land archipelago, arctic Russia – a literature review," in 1992 ICAM, 15–21.

Ershova, V., Prokopiev, A., Stockli, D., Kurapov, M., Kosteva, N., Rogov, M., et al. (2022). Provenance of the mesozoic succession of Franz Josef Land (north-eastern Barents Sea): paleogeographic and tectonic implications for the high arctic. *Tectonics* 41, 1–27. doi:10.1029/2022tc007348

Ettensohn, F. R. (1985). "The catskill delta complex and the acadian orogeny: a model," in *The catskill delta: geological society of America special paper 201*. Editors D. L. Woodrow and W. D. Sevon (Boulder, CO: Geological Society of America), 39–49.

Ettensohn, F. R. (1987). Rates of relative plate motion during the Acadian orogeny based on the spatial distribution of black shales. *J. Geol.* 95, 572–582. doi:10.1086/629150

Ettensohn, F. R. (1994). "Tectonic control on formation and cyclicity of major Appalachian unconformities and associated stratigraphic sequences," in *Tectonic and Eustatic controls on sedimentary cycles*. Editors J. M. Dennison and F. R. Ettensohn (Tulsa: SEPM), 4, 218–242.

Ettensohn, F. R. (2004). Modeling the nature and development of major paleozoic clastic wedges in the Appalachian Basin, USA. *J. Geodyn.* 37, 657–681. doi:10.1016/j.jog.2004.02.009

Ettensohn, F. R. (2008). "Chapter 4: the Appalachian foreland basin in eastern United States," in *The sedimentary basins of the United States and Canada: sedimentary basins of the world*. Editor A. Miall (Amsterdam: Elsevier), 105–179.

Ettensohn, F. R., Hohman, J. C., Kulp, M. A., and Rast, N. (2002). Evidence and implication of possible far-field responses to Taconian orogeny: Middle–Late Ordovician Lexington platform and Sebree trough, east-central United States. *Southeast. Geol.* 41, 1–36.

Ettensohn, F. R., and Lierman, R. T. (2015). "Using black shales to constrain possible tectonic and structural influence on foreland-basin evolution and cratonic yoking: late Taconian Orogeny, Late Ordovician Appalachian Basin, eastern USA," in *Sedimentary basins and crustal processes at continental margins: from modern hyper-extended margins to deformed ancient analogues*. Editors G. M. Gibson, F. Roure, and G. Manatschal (London: Geological Society), 119–141. Special Publications, 413.

Ettensohn, F. R., Pashin, J. C., and Gilliam, W. (2019). "The appalachian and black warrior basins: foreland basins in the eastern United States," in *The sedimentary basins of the United States and Canada: sedimentary basins of the world*. Editor A. Miall (Amsterdam: Elsevier), 129–237.

Faleide, J. I., Pease, V., Curtis, M., Klitzke, P., Minakov, A., Scheck-Wenderoth, M., et al. (2017). "Tectonic implications of the lithospheric structure across the Barents and Kara shelves," in *Circum-arctic lithosphere evolution*. Editors V. Pease and B. Coakley (London: Geological Society of London), 285–314. Special Publications, 460.

Filatova, N. I., and Khain, V. E. (2010). The Arctida craton and Neoproterozoic–Mesozoic orogenic belts of the circum–polar region. *Geotectonics* 44, 203–227. doi:10.1134/s0016852110030015

Fleming, E. J., Flowerdew, M. J., Smyth, H. R., Scott, R. A., Morton, A. C., Omma, J. E., et al. (2016). Provenance of Triassic sandstones on the southwest Barents Shelf and the implication for sediment dispersal patterns in northwest Pangaea. *Mar. Petroleum Geol.* 78, 516–535. doi:10.1016/j.marpetgeo.2016.10.005

Gabrielsen, R. H., Færseth, R. B., Jensen, L. N., Kalheim, J. E., and Fridtjof, R. (1990). Structural elements of the Norwegian continental shelf. Pt. 1. *Barents Region Nor. Petroleum Dir.* 6, 123–135.

Gac, S., Huismans, R. S., Simon, N. S. C., Podladchikov, Y. Y., and Faleide, J. I. (2013). Formation of intracratonic basins by lithospheric shortening and phase changes: a case study from ultra-deep East Barents Sea basin. *Terra Nova.* 25, 459–463. doi:10.1111/ter.12057

Garcia-Castellanos, D., Fernandez, M., and Torne, M. (1997). Numerical modeling of foreland basin formation: a program relating thrusting, flexure, sediment geometry and lithosphere rheology. *Comput. Geosciences* 23, 993–1003. doi:10.1016/s0098-3004(97)00057-5

Gavrilov, V. P., Gibshman, N. B., Karnaukhov, S. M., Kholodilov, V. A., Tsemkalo, M. A., and Shamalov, Y. V. (2010). *Biostratigraphy and lithofacies oil and gas bearing deposits Barents-Kara Sea region*. Moscow: Nedra Publishing House, 255.

Gianni, G. M., García, H. P. A., Pesce, A., Lupari, M., González, M., and Giambiagi, L. (2020). Oligocene to present shallow subduction beneath the southern Puna plateau. *Tectonophysics* 780, 228402. doi:10.1016/j.tecto.2020.228402

Gilmullina, A., Klausen, T. G., Paterson, N. W., Suslova, A., and Eide, C. H. (2021). Regional correlation and seismic stratigraphy of Triassic strata in the greater Barents Sea: implications for sediment transport in Arctic basins. *Basin Res.* 33, 1546–1579. doi:10.1111/bre.12526

Glørstad-Clark, E., Faleide, J. I., Lundschien, B. A., and Nystuen, J. P. (2010). Triassic seismic sequence stratigraphy and paleogeography of the western Barents Sea area. *Mar. Petroleum Geol.* 27, 1448–1475. doi:10.1016/j.marpetgeo.2010.02.008

Grogan, P., Østvedt-Ghazi, A.-M., Larssen, G. B., Fotland, B., Nyberg, K., Dahlgren, S., et al. (1999). "Structural elements and petroleum geology of the Norwegian sector of the northern Barents Sea," in *Petroleum geology of northwest Europe: proceedings of the 5th conference*. Editors A. J. Fleet and S. A. R. Boldy (London: the Geological Society), 1, 247–259.

Gudlaugsson, S. T., Faleide, J. I., Johansen, S. E., and Breivik, A. J. (1998). Late palaeozoic structural development of the south-western Barents Sea. *Mar. Petroleum Geol.* 15, 73–102. doi:10.1016/s0264-8172(97)00048-2

Hassaan, M., Faleide, J. I., Gabrielsen, R. H., and Tsikalas, F. (2020). Carboniferous graben structures, evaporite accumulations and tectonic inversion in the southeastern Norwegian Barents Sea. *Mar. Petroleum Geol.* 112, 104038. doi:10.1016/j.marpetgeo.2019.104038

Hatcher, R. D., Jr. (2010). "The Appalachian orogen: a brief summary," in *From rodinia to pangea: the lithotectonic record of the appalachian region*. Editors R. P. Tollo, M. J. Bartholomew, J. P. Hibbard, and P. M. Karabinos (Boulder, CO: Geological Society of America Memoir), 1–19.

Henriksen, E., Kvamme, L., and Rydningen, T. A. (2023). "Hammerfest Basin composite tectono-sedimentary element, Barents Sea," in *Sedimentary successions in the Arctic region and their hydrocarbon prospectivity*. Editors S. S. Drachev, H. Brekke, E. Henriksen, and T. Moore (London: Geological Society), 1–35. Memoirs, v. 57.

Henriksen, E., Ryseth, A. E., Larssen, G. B., Heide, T., Rønning, K., Sollid, K., et al. (2011). "Tectonostratigraphy of the greater Barents Sea: implications for petroleum systems," in *Arctic petroleum geology*. Editors A. M. Spencer, A. F. Embry, D. L. Gautier, A. Stoupakova, and K. Sørensen (London: Geological Society, Memoirs), 163–195.

Indrevær, K., Gac, S., Gabrielsen, R. H., and Faleide, J. I. (2017). Crustal-scale subsidence and uplift caused by metamorphic phase changes in the lower crust: a model for the evolution of the Loppa High area, SW Barents Sea from late Paleozoic to Present. *J. Geol. Soc.* 175, 497–508. doi:10.1144/jgs2017-063

Jamieson, R. A., and Beaumont, C. (1988). Orogeny and metamorphism: a model for deformation and pressure-temperature-time paths with applications to the central and southern Appalachians. *Tectonics* 7, 417–445. doi:10.1029/tc007i003p00417

Johansen, S. E., Ostisty, B. K., Birkeland, Ø., Federovsky, Y. F., Martirosjan, V. N., Bruun Christensen, O., et al. (1993). "Hydrocarbon potential in the Barents Sea region: play distribution and potential," in *Arctic geology and petroleum potential*. Editors T. O. Vorren, E. Bergsager, Ø. A. Dahl-Stamnes, E. Holter, B. Johansen, E. Lie, et al. (Amsterdam: Elsevier), 273–320.

Johnson, J. G. (1971). Timing and coordination of orogenic, epeirogenic, and eustatic events. *Geol. Soc. Am. Bull.* 82, 3263–3298. doi:10.1130/0016-7606(1971)82[3263:tacooe]2.0.co;2

Jordan, T. E. (1981). Thrust loads and foreland basin evolution, Cretaceous, Western United States. *AAPG Bull.* 65, 2506–2520. doi:10.1306/03b599f4-16d1-11d7-8645000102c1865d

Karner, G. D., and Watts, A. B. (1983). Gravity anomalies and flexure of the lithosphere at mountain ranges. *J. Geophys. Res.* 88 (10), 10449–10477. doi:10.1029/jb088ib12p10449

Kempf, O., and Pfiffer, O. A. (2004). Early Tertiary evolution of the north Alpine foreland basin of the Swiss Alps and adjoining areas. *Basin Res.* 16, 549–567. doi:10.1111/j.1365-2117.2004.00246.x

Khudoley, A. K., Sobolev, N. N., Petrov, E. O., Ershova, V. B., Makariev, A. A., Makarieva, E. V., et al. (2019). A reconnaissance provenance study of Triassic–Jurassic clastic rocks of the Russian Barents Sea. *GFF* 141, 263–271. doi:10.1080/11035897.2019.1621372

Klausen, T. G., Müller, R., Poyatos-Moré, M., Olaussen, S., and Stueland, E. (2022). Tectonic, provenance and sedimentological controls on reservoir characteristics in the upper triassic–middle jurassic realgrunnen subgroup, SW Barents Sea. *Geol. Soc. Lond. Special Publ.* 495, 237–261. doi:10.1144/sp495-2018-165

Klausen, T. G., Müller, R., Slama, J., and Helland-Hansen, W. (2016). Evidence for late triassic provenance areas and early jurassic sediment supply turnover in the Barents Sea Basin of northern pangea. *Lithosphere* 1, 14–28. doi:10.1130/l556.1

Klausen, T. G., Nyberg, B., and Helland-Hansen, W. (2019). The largest delta plain in Earth's history. *Geology* 47, 470–474. doi:10.1130/g45507.1

Klausen, T. G., Ryseth, A. E., Helland-Hansen, W., Gawthorpe, R., and Laursen, I. (2014). Spatial and temporal changes in geometries of fluvial channel bodies from the Triassic Snadd Formation of offshore Norway. *J. Sediment. Res.* 84, 567–585. doi:10.2110/jsr.2014.47

Klausen, T. G., Ryseth, A. E., Helland-Hansen, W., Gawthorpe, R., and Laursen, I. (2015). Regional development and sequence stratigraphy of the Middle to late triassic snadd formation, Norwegian Barents Sea. *Nor. Barents Sea Mar. Petroleum Geol.* 62, 102–122. doi:10.1016/j.marpetgeo.2015.02.004

Klein, G. D. (1994). "Depth determination and quantitative distinction of the influence of tectonic subsidence and climate on changing sea level during deposition of Mid-continent Pennsylvanian cyclothems," in *Tectonic and eustatic controls on sedimentary cycles*. Editors J. M. Dennison and F. R. Ettensohn (SEPM Concepts in Sedimentology and Paleontology), 35–50.

Klein, G. V., and Hsui, A. T. (1987). Origin of cratonic basins. *Geology* 15, 1094–1098. doi:10.1130/0091-7613(1987)15<1094:oocb>2.0.co;2

Klitzke, P., Franke, D., Ehrhardt, A., Lutz, R., Reinhardt, L., Heyde, I., et al. (2019). The paleozoic evolution of the Olga Basin region, northern Barents Sea: a link to the timanian orogeny. *Geochem. Geophys. Geosystems* 20, 614–629. doi:10.1029/2018gc007814

Korago, E. A., Kovaleva, G. N., Il'in, V. F., and Pavlov, L. G. (1992). *The tectonics and metallogeny of the early kimmerides of Novaya Zemlya*. St. Petersburg: Nedra, 203. (in Russian).

Kruse, S., and McNutt, M. (1988). Compensation of paleozoic orogens: a comparison of the urals to the appalachians. *Tectonophysics* 154, 1–17. doi:10.1016/0040-1951(88)90224-7

Lerch, B., Karlsen, D. A., Abay, T. B., Duggan, D., Seland, R., and Backer-Owe, K. (2016). Regional petroleum alteration trends in Barents Sea oils and condensates as a clue to migration regimes and processes. *AAPG Bull.* 2, 165–190. doi:10.1306/08101514152

Line, L. H., Müller, R., Klausen, T. G., Jahren, J., and Hellevang, H. (2020). Distinct petrographic responses to basin reorganization across the Triassic–Jurassic boundary in the southwestern Barents Sea. *Basin Res.* 32, 1463–1484. doi:10.1111/bre.12437

Lopatin, B. G., Pavlov, L. G., Orgo, V. V., and Shkarubo, S. I. (2001). Tectonic structure of Novaya Zemlya. *Polarforschung* 69, 131–135.

Lord, G. S., Mørk, M. B. E., Mørk, A., and Olaussen, S. (2019). Sedimentology and petrography of the Svenskøya Formation on hopen, svalbard: an analogue to sandstone reservoirs in the realgrunnen subgroup. *Polar Res.* 38, 1–24. doi:10.33265/polar.v38.3523

Lord, G. S., Solvi, K. H., Klausen, T. G., and Mørk, A. (2014). Triassic channel bodies on Hopen, Svalbard: their facies, stratigraphic significance, and spatial distribution. *Nor. Pet. Dir.* 11, 41–59.

Lundschien, B. A., Høy, T., and Mørk, A. (2014). Triassic hydrocarbon potential in the northern Narents Sea; integrating Svalbard and stratigraphic core data. *Nor. Pet. Dir. Bull.* 11, 3–20.

Lundschien, B. A., Mattingsdal, R., Johansen, S. K., and Knutsen, S.-M. (2023). "North Barents composite tectono-sedimentary element," in *Sedimentary successions in the Arctic region and their hydrocarbon prospectivity*. Editors S. S. Drachev, H. Brekke, E. Henriksen, and T. Moore (London: Geological Society), 1–16. Memoirs, v. 57.

Margulis, E. A. (2009). Evolution of the Barents Sea region and its hydrocarbon systems. *Neft. Geol. Teor. I Pract.* 4, 1–14.

Martins, G., Ettensohn, F., and Knutsen, S.-M. (2022). The Appalachian area as a tectonostratigraphic analogue for the Barents Sea shelf. *Basin Res.* 34, 274–299. doi:10.1111/bre.12619

Martins, G., Ettensohn, F., and Knutsen, S.-M. (2023). Use of backstripping in the Triassic–Middle Jurassic, south-central Barents Sea shelf succession to understand regional tectonic mechanisms and structural responses. *Tectopnophysics* 853, 229797. doi:10.1016/j.tecto.2023.229797

McKerrow, W. S., Mac Niocaill, C., and Dewey, J. F. (2000). The caledonian orogeny redefined. *J. Geol. Soc.* 157, 1149–1154. doi:10.1144/jgs.157.6.1149

Merschat, A. J., and Hatcher, R. D., Jr. (2007). "The Cat Square terrane: Possible Silurian-Devonian remnant ocean basin in the Inner Piedmont, Southern Appalachians, U.S.A." in *4-D framework of continental crust*. Editors R. D. HatcherJr., M. P. Carlson, J. H. McBride, and J. R. Martínez Catalan (Geological Society of America Memoir 200), 1252–1281.

Miall, A. D. (1997). *The geology of stratigraphic sequences*. Berlin: Springer, 433.

Mørk, A. (1999). Compositional variations and provenance of Triassic sandstones from the Barents Shelf. *J. Sediment. Res.* 69, 690–710. doi:10.2110/jsr.69.690

Mørk, A., Dallmann, W. K., Dypvik, H., Johannessen, E. P., Larssen, G. B., Nagy, J., et al. (1999). "Mesozoic lithostratigraphy," in *Lithostratigraphic lexicon of Svalbard. Upper Palaeozoic to Quaternary bedrock. Review and recommendations for nomenclature use*. Editor W. K. Dallmann (Tromsø: Norsk Polarinstitutt), 127–214.

Mørk, A., Embry, A. F., and Weitschat, W. (1989). "Triassic transgressive–regressive cycles in the Sverdrup Basin, Svalbard and the Barents Sea shelf," in *Correlation in hydrocarbon exploration*. Editor J. D. Collinson (Bergen: Graham and Trotman), 113–130.

Müller, R., Klausen, T. G., Faleide, J. I., Olaussen, S., Eide, C. H., and Suslova, A. (2019). Linking regional unconformities in the Barents Sea to compression-induced forebulge uplift at the Triassic-Jurassic transition. *Tectonophysics* 765, 35–51. doi:10.1016/j.tecto.2019.04.006

Müller, R., Klausen, T. G., Line, L. H., Hafeez, A., Planke, S., Eide, F., et al. (2022). Tectonostratigraphic development of the Upper Triassic to Middle Jurassic in the Hoop Area, Barents Sea: Implications for understanding ultra-condensed reservoir units. *Mar. Petroleum Geol.* 145, 105787. doi:10.1016/j.marpetgeo.2022.105787

Nikishin, A. M., Ziegler, P. A., Stephenson, R. A., Cloetingh, S. A. P. L., Furne, A. V., Fokin, P. A., et al. (1996). Late Precambrian to Triassic history of the East European Craton: Dynamics of sedimentary basin evolution. *Tectonophysics* 268, 23–63. doi:10.1016/s0040-1951(96)00228-4

Nikishin, V. A., Malyshev, N. A., Nikishin, A. M., and Obmetko, V. V. (2011). The Late Permian–Triassic system of rifts of the South Kara sedimentary basin. *Mosc. Univ. Geol. Bull.* 66, 377–384. doi:10.3103/s0145875211060093

Norina, D. A., Stupakova, A. V., and Kiryukhina, T. A. (2014). Depositional environments and the hydrocarbon generative potential of Triassic rocks of the Barents Sea basin. *Mosc. Univ. Geol. Bull.* 69, 1–10. doi:10.3103/s0145875214010062

Norwegian Petroleum Directorate (NPD) (2023). *Fact Pages*. Norwegian Petroleum Directorate. Available from: https://factpages.npd.no/en/strat.

Olaussen, S., Grundvåg, S.-A., Senger, K., Anell, I., Betlem, P., Birchall, T., et al. (2022). The Svalbard Carboniferous to Cenozoic composite tectono-stratigraphic element. *Geol. Soc.* 57, 1–65. doi:10.1144/m57-2021-36

Olaussen, S., Larssen, G. B., Helland-Hansen, W., Johannessen, E. P., Nøttvedt, A., Riis, F., et al. (2018). Mesozoic strata of Kong Karls Land, Svalbard, Norway; a link to the northern Barents Sea basins and platforms. *Nor. J. Geol.* 98, 1–70. doi:10.17850/njg98-4-06

Otto, S. C., and Bailey, R. J. (1995). Tectonic evolution of the northern Ural Orogen. *J. Geol. Soc.* 152, 903–906. doi:10.1144/gsl.jgs.1995.152.01.03

Parizot, O., Missenard, Y., Vergely, P., Haurine, F., Noret, A., Delpech, G., et al. (2020). *Tectonic record of deformation in intraplate domains: case study of far-field deformation in the Grands Causses area*. France: Geofluids, 1–19.

Paterson, N. W., and Mangerud, G. (2017). Palynology and depositional environments of the Middle–Late Triassic (Anisian–Rhaetian) Kobbe, Snadd and Fruholmen formations, southern Barents Sea, Arctic Norway. *Mar. Petroleum Geol.* 86, 304–324. doi:10.1016/j.marpetgeo.2017.05.033

Paterson, N. W., and Mangerud, G. (2019). A revised palynozonation for the Middle–Upper Triassic (Anisian–Rhaetian) series of the Norwegian Arctic. *Geol. Mag.* 157, 1568–1592. doi:10.1017/s0016756819000906

Paterson, N. W., Mangerud, G., Cetean, C. G., Mørk, A., Lord, G. S., Klausen, T. G., et al. (2016). A multidisciplinary biofacies characterisation of the Late Triassic (late Carnian–Rhaetian) Kapp Toscana Group on Hopen, Arctic Norway. *Palaeogeogr. Palaeoclimatol. Palaeoecol.* 464, 16–42. doi:10.1016/j.palaeo.2015.10.035

Petrov, O. V., Sobolev, N. N., Koren, T. N., Vasiliev, V. E., Petrov, E. O., Larssen, G. B., et al. (2008). Palaeozoic and Early Mesozoic evolution of the East Barents and Kara Seas sedimentary basins. *Nor. J. Geol.* 88, 227–234.

Polyakova, I. D. (2015). Petroleum source rocks of the arctic region. *Lithology Mineral Resour.* 50, 26–49. doi:10.1134/s002449021406008x

Posamentier, H. W., and Morris, W. R. (2000). Aspects of the stratal architecture of forced regressive deposits. *Geol. Soc. Lond.* 172, 19–46. doi:10.1144/gsl.sp.2000.172.01.02

Puchkov, V. N. (2002). "Paleozoic evolution of the East European continental margin involved in the Uralide Orogeny," in *Mountain building in the uralides*. Editors D. Brown, C. Juhlin, and V. Puchkov (Washington DC: American Geophysical Union, Geophysical Monograph), 9–31.

Puchkov, V. N. (2009). The evolution of the Uralian orogen. *Geol. Soc. Lond. Spec. Publ.* 327, 161–195. doi:10.1144/sp327.9

Quinlan, G. M., and Beaumont, C. (1984). Appalachian thrusting, lithospheric flexure, and the Paleozoic stratigraphy of the eastern interior of North America. *Can. J. Earth Sci.* 21, 973–996. doi:10.1139/e84-103

Riis, F., Lundschien, B. A., Høy, T., Mørk, A., and Mørk, M. B. (2008). Evolution of the Triassic shelf in the northern Barents Sea region. *Polar Res.* 27, 318–338. doi:10.1111/j.1751-8369.2008.00086.x

Rismyhr, B., Bjærke, T., Olaussen, S., Mulrooney, M. J., and Senger, K. (2019). Facies, palynostratigraphy and sequence stratigraphy of the Wilhelmøya Subgroup (Upper Triassic–Middle Jurassic) in western central Spitsbergen, Svalbard. *Nor. J. Geol.* 99, 183–212. doi:10.17850/njg001

Ritzmann, O., and Faleide, J. I. (2009). The crust and mantle lithosphere in the Barents Sea/Kara Sea region. *Tectonophysics* 470, 89–104. doi:10.1016/j.tecto.2008.06.018

Roberts, D., and Siedlecka, A. (2002). Timanian orogenic deformation along the northeastern margin of Baltica, Northwest Russia and Northeast Norway, and Avalonian–Cadomian connections. *Tectonophysics* 353, 169–184. doi:10.1016/s0040-1951(02)00195-6

Ryseth, A. (2014). "Sedimentation at the Jurassic–Triassic boundary, south-west Barents Sea: indication of climate change," in *From Depositional systems to sedimentary successions on the Norwegian continental margin*. Editors W. Martinius, R. Ravnås, J. A. Howell, R. J. Steel, and J. P. Wonham (Chichester: International Association of Sedimentologists), 187–214.

Schenk, C. J. (2011). "Geology and petroleum potential of the Timan-Pechora basin province, Russia, The geological evolution and hydrocarbon potential of the Barents and Kara shelves," in *Arctic petroleum geology*. Editors A. M. Spencer, A. F. Embry, D. L. Gautier, A. V. Stoupakova, and K. Sørensen (London: The Geological Society of London Memoirs), 35, 283–294.

Scott, R. A., Howard, J. P., Guo, L., Schekoldin, R., and Pease, V. (2010). "Offset and curvature of the Novaya Zemlya fold-and-thrust belt, Arctic Russia," in *Petroleum geology: from mature basins to new Frontiers – proceedings of the 7th petroleum geology conference*. Editors B. A. Vining and S. C. Pickering (London: The Geological Society, Petroleum Geology Conferences), 645–657.

Shkarubo, S. I., Burguto, A. G., Zuykova, O. N., Kostin, D. A., Velichko, B. M., Zhuravlev, V. A., et al. (2017). *State geological map of the Russian federation (in Russian): saint petersburg, VSEGUEI, The North-Kara-Barents sea series, sheets S-38, scale 1: 1,000,000*.

Sinclair, H. D., Coakley, B. J., Allen, P. A., and Watts, A. B. (1991). Simulation of foreland basin stratigraphy using a diffusion model of mountain belt uplift and erosion: an example from the central Alps, Switzerland. *Tectonics* 10, 599–620. doi:10.1029/90tc02507

Smelror, M., and Petrov, O. V. (2018). Geodynamics of the Arctic: From Proterozoic orogens to present day seafloor spreading. *J. Geodyn.* 121, 185–204. doi:10.1016/j.jog.2018.09.006

Smelror, M., Petrov, O. V., Larssen, G. B., and Werner, S. C. (2009). *Geological history of the Barents Sea: trondheim*. Trondheim, Norway: Geological Survey of Norway, 135.

Sobornov, K. (2022). Korotaikha composite tectono-sedimentary element, Northwestern Russia. *Geol. Soc.* 57, 2–15. doi:10.1144/m57-2018-28

Sobornov, K. O., and Astafiev, D. A. (2017). Structure, formation and oil and gas potential of the northern part of the Korothaika depression, Barents Sea. *Vesti Gazov. Nauki* 4, 25–37.

Sømme, T. O., Doré, A. G., Lundin, E. R., and Tørudbakken, B. O. (2018). Triassic–Paleogene paleogeography of the Arctic: Implications for sediment routing and basin fill. *AAPG Bull.* 102, 2481–2517. doi:10.1306/05111817254

Spina, V., Borgomano, J., Nely, G., Shchukina, N., Irving, A., Neumann, C., et al. (2015). Characterization of the Devonian Kharyaga carbonate platform (Russia): Integrated and multiscale approach. *AAPG Bull.* 99, 1771–1799. doi:10.1306/03031514119

Stemmerik, L. (2000). Late Palaeozoic evolution of the North Atlantic margin of Pangea. *Palaeogeogr. Palaeoclimatol. Palaeoecol.* 161, 95–126. doi:10.1016/s0031-0182(00)00119-x

Stemmerik, L., and Worsley, D. (2005). 30 years on – Arctic Upper Palaeozoic stratigraphy, depositional evolution and hydrocarbon prospectivity. *Nor. J. Geol.* 85, 151–168.

Stoupakova, A. V., Henriksen, E., Burlin, Yu.K., Larsen, G. B., Milne, J. K., Kiryukhina, T. A., et al. (2011). "The geological evolution and hydrocarbon potential of the Barents and Kara shelves," in *Arctic petroleum geology*. Editors A. M. Spencer, A. F. Embry, D. L. Gautier, A. V. Stoupakova, and K. Sørensen (London: The Geological Society of London), 325–344. Memoirs, v. 35.

Su, W., Huff, W. D., Ettensohn, F. R., Liu, X., Zhang, J., and Li, Z. (2009). K-bentonite, black-shale and flysch successions at the Ordovician-Silurian transition, South China: Possible sedimentary responses to the accretion of Cathaysia to the Yangtze Block and its implications for the evolution of Gondwana. *Gondwana Res.* 15, 111–130. doi:10.1016/j.gr.2008.06.004

Suslova, A. A. (2014). Seismostratigraphic analysis and petroleum potential prospects of Jurassic deposits, Barents Sea shelf. *Petroleum Geology-Theoretical Appl. Stud.* 9, 1–19. doi:10.17353/2070-5379/24_2014

Suslova, A. A., Stoupakova, A. V., Mordasova, A. V., Sautkin, R. S., and Gilmullina, A. A. (2021). Structural reconstructions of the Eastern Barents Sea at Meso-Tertiary evolution and influence on petroleum potential. *Georesources* 23, 78–84. doi:10.18599/grs.2021.1.8

Torsvik, T. H., and Cocks, L. R. M. (2017). *Earth history and palaeogeography*. Cambridge: Cambridge University Press, 324.

Uchman, A., Hanken, N.-M., Nielsen, J. K., Grundvåg, S.-A., and Piasecki, S. (2016). Depositional environment, ichnological features and oxygenation of Permian to earliest Triassic marine sediments in central Spitsbergen. *Svalbard Polar Res.* 35, 1–21. doi:10.3402/polar.v35.24782

Ussami, N., Shiraiwa, S., and Dominguez, J. M. L. (2010). Basement reactivation in a sub-Andean foreland flexural bulge: The Pantanal wetland, SW Brazil. *Tectonics* 18, 25–39. doi:10.1029/1998tc900004

Vail, P. R. (1987). Seismic stratigraphy interpretation using sequence stratigraphy: Part 1: Seismic stratigraphy interpretation procedure. *AAPG Spec. Vol.* 1, 1–10.

Vail, P. R., and Mitchum, R. M., Jr. (1977). "Seismic stratigraphy and global changes of sea level, part 1: Overview," in *Applications to hydrocarbon exploration*. Editor C. E. Payton (Ann Arbor: Edward Brothers), 26, 51–53.

Van Wagoner, J. C., and Bertram, G. T. (1995). *Sequence stratigraphy of foreland basin deposits: tulsa*. American Association of Petroleum Geologists, 490.

Worsley, D. (2008). The post-Caledonian development of Svalbard and the western Barents Sea. *Polar Res.* 27, 298–317. doi:10.1111/j.1751-8369.2008.00085.x

Zhang, X., Pease, V., Carter, A., and Scott, R. (2018). "Reconstructing Palaeozoic and Mesozoic tectonic evolution of Novaya Zemlya: combining geochronology and thermochronology," in *Circum-arctic lithosphere evolution*. Editors V. Pease and B. Coakley (London: The Geological Society, Special Publications), 335–353.

Ziegler, P. A. (1987). Late cretaceous and Cenozoic intraplate compressional deformations in the Alpine foreland—a geodynamic model. *Tectonophysics* 137, 389–420. doi:10.1016/0040-1951(87)90330-1

Ziegler, P. A. (1989). *Evolution of laurussia*. Dordrecht: Kluwer Academic Publishers, 102.

Ziegler, P. A., Bertotti, G., and Cloetingh, S. (2002). Dynamic processes controlling foreland development – the role of mechanical (de)coupling of orogenic wedges and forelands. *EGU Stephan Mueller Spec. Publ. Ser.* 1, 17–56. doi:10.5194/smsps-1-17-2002

Ziegler, P. A., Cloetingh, S., and van Jan-Diederik, W. (1995). Dynamics of intra-plate compressional deformation: the Alpine foreland and other examples. *Tectonophysics* 252, 7–59. doi:10.1016/0040-1951(95)00102-6